Hydrological, thermal and chemical influence of an intact rock glacier discharge on mountain stream water

Hydrological, thermal and chemical influence of an intact rock glacier discharge on mountain stream water

Bearzot, F.[1,2,*,†], Colombo, N.[3,4,†], Cremonese, E.[5], Morra Di Cella, U.[5], Drigo, E.[6], Caschetto, M.[1], Basiricò, S.[1], Crosta, G.B.[1], Frattini, P.[1], Freppaz, M.[4], Pogliotti, P.[5], Salerno, F.[7], Brunier, A.[5], Rossini, M.[1]

[1]Department of Earth and Environmental Sciences, University of Milano-Bicocca, Piazza della Scienza 1, 20126, Milan, Italy.

[2]Faculty of Science and Technology, Free University of Bozen-Bolzano, Piazza Università 1, 39100, Bozen, Italy.

[3]Water Research Institute, National Research Council of Italy, Rome, Italy.

[4]Department of Agricultural, Forest and Food Sciences, University of Turin, Grugliasco, Italy.

[5]Environmental Protection Agency of Valle d'Aosta, Climate Change Unit, Saint-Christophe, Italy.

[6]Geologist freelance.

[7]Institute of Polar Sciences, National Research Council of Italy, Milan, Italy.

*Corresponding author: *francesca.bearzot@unibz.it*

†These authors equally contributed to the paper.

Abstract

Rock glaciers are the most prominent permafrost-related mountain landforms. This study investigates the effects of the discharge from an intact rock glacier on the hydrological, thermal and chemical dynamics of a high-elevation stream in the NW Italian Alps. Despite draining only 39% of the watershed area, the rock glacier sourced a disproportionately large amount of discharge to the stream, with the highest relative contribution to the catchment streamflow occurring in late summer - early autumn (up to 63%). However, ice melt was estimated to be only a minor component to the discharge of the rock glacier, due to its insulating coarse debris mantle. The sedimentological characteristics and internal hydrological system of the rock glacier played a major role in its capability to store and transmit relevant amounts of groundwater, especially during the baseflow periods. Besides the hydrological influence, the cold and solute-enriched discharge from the rock glacier significantly lowered the stream water temperature (especially during warm atmospheric periods) as well as increased the concentrations of most solutes in the stream. Furthermore, in the two lobes forming the rock glacier, different internal hydrological systems, likely driven by different permafrost and ice content, caused contrasting hydrological and chemical behaviours. Indeed, higher hydrological contributions and significant seasonal trends in solute concentrations were found in the lobe with higher permafrost and ice content, due to different flowpaths. Our results highlight the relevance of rock glaciers as water resources, despite the minor ice melt contribution, also suggesting their potential, increasing hydrological importance in the light of climate warming.

Keywords: rock glaciers, hydrology, permafrost, discharge, water chemistry, climate change

1. Introduction

Billions of people depend on water supply from mountain regions (Viviroli et al., 2020), where climate change is driving a shift in precipitation phase from snow to rain and a trend toward earlier snowmelt (Huss et al., 2017). At the same time, mountain glaciers around the world are rapidly receding (e.g., Hugonnet et al., 2021; Zemp et al., 2015), shifting the predominant dynamics of the mountain cryosphere from glacial to periglacial (e.g., Haeberli et al., 2017; Seppi et al., 2015). This shift could have relevant implications for mountain water resources (e.g., Arenson et al., 2022; Wagner et al., 2021a). For instance, the projection of ice loss rates indicates that in the next decades more subsurface ice may remain compared to glacier surface ice, due to their different response times to atmospheric changes (Arenson et al., 2022; Haeberli et al., 2017). In turn, permafrost degradation and subsurface ice loss may partially offset water shortages by increasing the water storage capacity of mountain terrains due to the increase in the unfrozen sediment thickness (Rogger et al., 2017).

Rock glaciers are the most prominent permafrost-related mountain landforms (Haeberli et al., 2006). Intact rock glaciers consist of a seasonal frozen layer (active layer) covering ice-supersaturated debris and/or pure ice (Jones et al., 2019), differing from relict rock glaciers which do not longer contain ice (Haeberli et al., 2006). Intact rock glaciers can store water in solid (ice/snow) and liquid form (groundwater) (Wagner et al., 2021a), potentially representing a relevant water source under future climate warming conditions (Arenson et al., 2022; Jin et al., 2022; Jones et al., 2018). Rock glacier water storage occurs at long-term (ice storage from multiannual to millennial timescales), intermediate-term (snow storage and release of water on seasonal timescales) and short-term timescales (water diurnal drainage) (Jones et al., 2019). Despite the increasing attention gained by intact rock glaciers as water sources, their contribution to the runoff of high-elevation catchments, and its seasonal variations, remain largely unexamined.

Discharge from intact rock glaciers usually originates from snowpack and internal ice melting, rainfall, and groundwater (Krainer et al., 2007). Commonly, the highest discharge rates occur during the spring - early summer snowmelt, and gradually decrease through summer and autumn with the lowest flow rates recorded in the winter months (Krainer and Mostler, 2002). In this framework, the identification and quantification of the contribution of the different water sources composing the discharge of intact rock glaciers is still unclear (cf., Krainer et al., 2007; Williams et al., 2006), above all the permafrost-ice melt rate and its contribution to the

water budget. In addition, irrespective of the water source, due to their cold discharge (Millar et al., 2013; Krainer et al., 2007; Krainer and Mostler, 2002), rock glaciers are also emerging as potential climate refugia, enabling the near- and long-term persistence of cold habitats and related biodiversity (Brighenti et al., 2021a). However, how cold waters emerging from intact rock glaciers can influence the thermal regime of high-elevation surface waters remains poorly investigated.

The degradation of permafrost and ice melting in rock glaciers can also affect the chemical characteristics of surface water (Colombo et al., 2018b). High content of solutes, such as ions, nutrients, and trace elements have been reported in intact rock glacier outflows (Brighenti et al., 2019; Colombo et al., 2019; 2018c; Williams et al., 2007; 2006). This occurrence has been also shown to impact the ecological conditions of downstream water bodies (Mania et al., 2018; Thies et al., 2013) and even the suitability of surface waters downstream of rock glaciers for use as safe, potable water sources (Ilyashuk et al., 2018; 2014). Despite the increasing number of studies devoted to the analysis of intact rock glacier hydrochemistry (Jones et al., 2019; Colombo et al., 2018a), it is evident that further scientific investigation is required, particularly focused on the quantification of the hydrochemical influence of intact rock glaciers on downstream water bodies.

The aim of this research is to assess the hydrological, thermal and chemical influence of an intact rock glacier discharge on high-elevation stream water in the NW Italian Alps (Valtournenche Valley, Aosta Valley). The specific objectives are to: (i) quantify the rock glacier hydrological influence (including the internal ice melt rate), and its seasonal variations, on the hydrologic stream regime; (ii) investigate how the rock glacier discharge thermally and chemically influences the stream water.

2. Study area

The study area is located in the NW Italian Alps, at the head of the Valtournenche Valley (Aosta Valley), in the south-eastern side of the Cervinia basin (Fig. 1a). The study is focused on the intact Gran Sometta Rock Glacier, a tongue-shaped landform originating from the rock walls of the Gran Sometta Peak (3165 m a.s.l.). The rock glacier is approximately 400-m long, between 150- and 300-m wide, with a thickness of 20–30 m, extending in elevation from 2630 to 2770 m a.s.l. (Bearzot et al., 2022).

The surface of the rock glacier consists of longitudinal ridges in the extensive central part, and a complex of transverse ridges and furrows in the compressive terminal part (Fig. 1). The debris cover is composed of

pebbles and angular blocks, in most places lacking any visible fine-grained matrix. Two adjacent lobes constitute the main body of the rock glacier, called “Black” and “White”, given their different colours, driven by the lithological composition. Indeed, the Black lobe is mainly composed of calcschists, with a secondary presence of dolomitic marbles and metabasites. The White lobe is primarily composed of dolomitic marbles, with a secondary presence of calcschists and metabasites. The remaining part of the study area is lithologically similar to the rock glacier. Bare cliffs and debris talus deposits are dominant outside the rock glacier, while soil cover with alpine meadows can be found in restricted areas, especially along the main stream draining the catchment, the Pousset stream.

The two rock glacier lobes differ in terms of internal structure and surface velocities (Bearzot et al., 2022). The internal structure of the White lobe is composed by two high-resistivity bodies in the central (30-m thickness) and terminal (20-m thickness) parts of the tongue, which are interpreted as substantial frozen ground occurrences. These parts are overlaid by a less resistive layer representing the active layer and, below, by resistivity values < 5 kohm m indicating unfrozen conditions. This lobe moves downstream at an average annual surface velocity of 0.5 m y^{-1}. The Black lobe displays a different internal structure, showing a continuous layer (20-m thickness) with high resistivity values (~100 kohm m) under the active layer, indicating a higher frozen ground content with respect to the White lobe. This lobe moves downstream at a velocity of about 1 m y^{-1}, twice as fast as the White lobe, likely due to its higher frozen ground content and, possibly, slightly different topographic conditions (Bearzot et al., 2022).

Two springs are located at the fronts of the lobes, discharging into the main stream. In the studied watershed (1.32 km^2), three hydrological catchments were outlined using the surface topography (2m×2m-cell digital terrain model), named “Up site” (upstream of the rock glacier), “White lobe”, and “Black lobe” (the last two related to the studied rock glacier lobes), draining 61% (0.80 km^2), 26% (0.34 km^2), and 13% (0.17 km^2) of the watershed area, respectively (Fig. 1a).

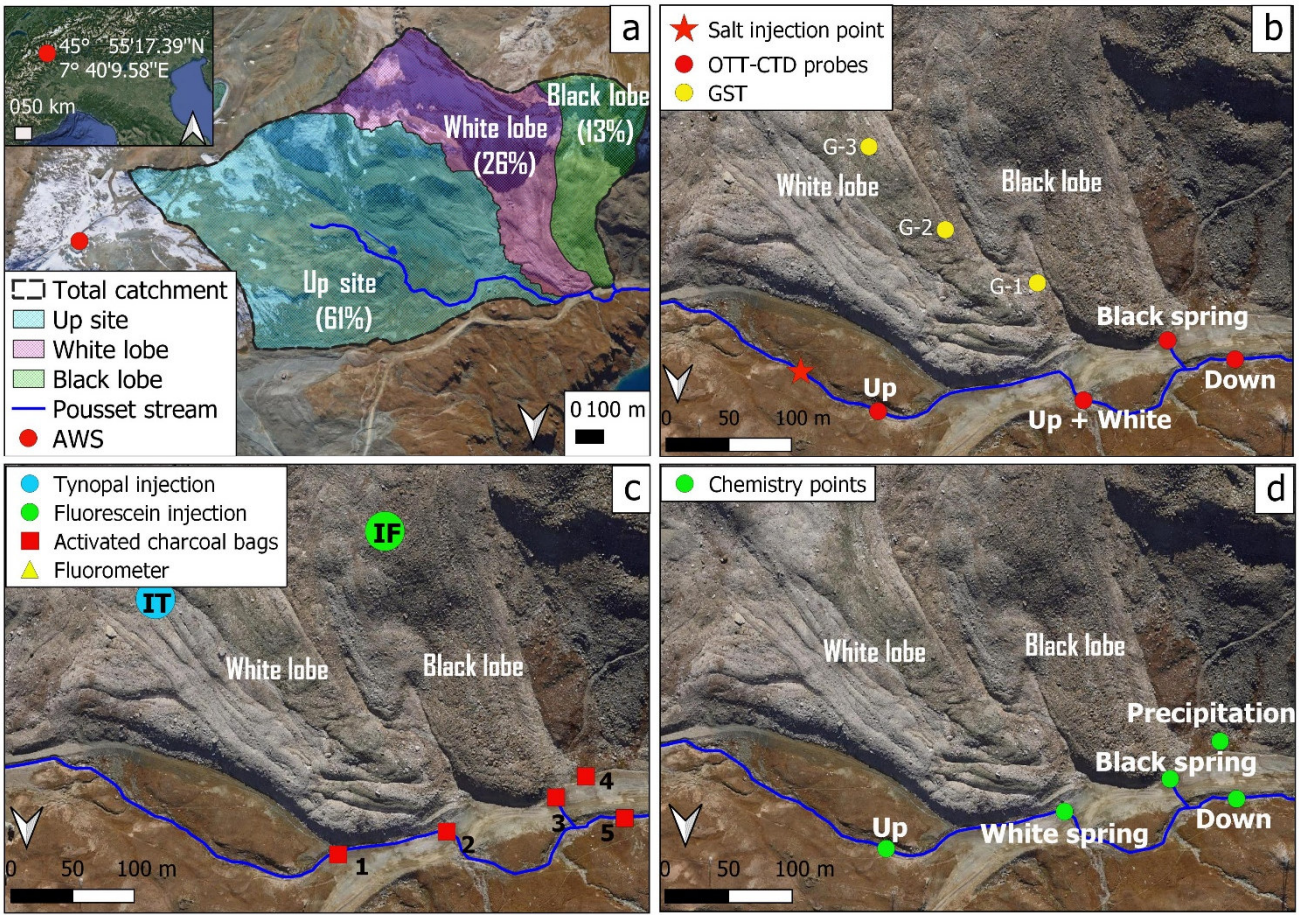

Figure 1. (a) Overview map of the study area, showing the sub-basin divisions with the respective planar-area contribution to the total catchment (%), the location of the Cime Bianche AWS, and the location of the study area in northern Italy (inset) (coordinate system: WGS84). Detailed view of the rock glacier measuring and sampling points: (b) three ground surface temperature (GST) data loggers, salt injection point, four sites equipped for the measurement of the discharge through the salt-dilution method, and locations of the probes; (c) five activated charcoal points, one field fluorometer, and two dye injection points; (d) isotopic and water chemistry sampling sites (the sampling point "Snow" is not shown since it is placed further upstream).

3. Data and methods

3.1 Meteorological conditions and snow-cover duration

A high-elevation automatic weather station (AWS) is located about 1 km West from the rock glacier front, the Cime Bianche AWS (3100 m a.s.l.) (Fig. 1a). For the time span 2010–2021, the mean annual air temperature was –2.6±0.9 °C. In summer (June, July, and August), the mean air temperature was around +4.4±1.8 °C. The snowpack generally developed by early-October, and the melt out of snow occurred around July. The mean maximum snow depth was 1.8±0.3 m. The liquid precipitation during the snow-free season

(no snow on the ground) was 262±138 mm on average. To support the investigations in the years 2019-2020-2021, daily air temperature, snow-depth and precipitation data from the Cime Bianche AWS were analysed.

Snow-cover duration in the catchment and on the rock glacier was estimated using two approaches with different spatial and temporal resolutions in order to adequately assess the presence/absence of snow in the main stream catchment and in-between the coarse debris on the rock glacier surface. To provide an estimate of the snow-covered area evolution in the entire basin, the Fractional Snow Cover (FSC) product (Dumont et al., 2021) of the Copernicus High Resolution Snow & Ice Monitoring Service (https://land.copernicus.eu/pan-european/buophysical-parameters/high-resolution-snow-and-ice-monitoring) was used. To analyse long-lasting snow among the coarse blocks on the rock glacier surface, miniature temperature sensors were installed to monitor snowmelt based on ground surface temperature (GST). Three temperature data loggers (Geotest AG, Switzerland) were installed on the rock glacier surface (*G-1*, *G-2*, and *G-3*, Fig. 1b), measuring GST up to a depth of 10 cm. Data were acquired every two hours between August 2018 and August 2021. The melt-out date of snow was calculated based on the daily standard deviation of GST, following Schmid et al. (2012).

3.2 Discharge measurements and water temperature

Discharge measurements were performed using NaCl as a chemical tracer (Hudson and Fraser, 2008). Tracer tests were carried out two times in 2019 (11th July and 3rd October), and approx. on a bi-weekly basis during the field summer seasons 2020 (3rd July 2020 – 30th September, 7 observations) and 2021 (9th July – 14th October, 9 observations). One injection point and three downstream measuring points were set (Fig. 1b). The downstream points were chosen to quantify the hydrological contribution from the rock glacier to the entire catchment runoff. Specifically, the point *Up* was located downstream of the injection point and upstream of the rock glacier, along the main stream; it was selected to quantify the water flow from the upstream catchment. The point *Up+White* was placed downstream of the White lobe tributary, in the main stream, to quantify the water flow given by the sum of the White lobe and *Up* site contributions. The third measuring point, *Down* (downstream), enclosed all the contributions from upstream (i.e., White and Black lobes, and *Up* site). In these selected points, three OTT-CTD probes (OTT HydroMet) were installed in 2020 and 2021 to continuously record physical and chemical parameters (water pressure, electrical conductivity - EC, and temperature) every 30 minutes throughout the investigated period and every 10 seconds only when the tracer

test was performed. A fourth probe was placed in the spring at the front of the Black lobe (*Black spring*, Fig. 1b). The White lobe spring (*White spring*) was not instrumented due to the very low superficial flow rate and tortuosity among the boulders, which did not allow the proper positioning of the probe. Several problems affected the installed OTT-CTD probes, mainly due to the low water level and occasionally fine sediment deposition, often resulting in erroneous readings. The water temperature data series was the only one that provided usable, continuous values, although not covering entirely the periods of investigation. Therefore, the discharge patterns were investigated only using the salt dilution approach (discrete measurements) and the chemical characteristics were analysed only based on grab samples.

3.3 Tracer tests

Tracer tests were performed to investigate the internal hydrological mechanisms and the potentially different storage and flow dynamics of the two lobes. The injections were carried out in a debris covered zone and in absence of snow-cover. Tynopal and fluorescein were injected on the surface of the rock glacier at the injection points *IT* and *IF* (Fig. 1c) on 23rd July 2021, at 11.00 am and 11.40 am, respectively. *IT* was injected at ca. 2710 m a.s.l. on the White lobe, and *IF* at 2735 m a.s.l. on the Black lobe. 200 g of tynopal and 50 g of fluorescein were injected and rinsed using 1000-l water tanks at the *IT* and *IF* points, respectively. After the tracer injections, the springs were monitored using activated charcoal and a field fluorometer capable to measure, in continuous, three tracers (Tynopal CBS-X, Na-fluorescein and any molecule in the rhodamine family) and turbidity (Schnegg, 2002).

Activated charcoal (10 g) was inserted in perforated bags, allowing water to seep through them. The dye tracer in the seeping water is absorbed cumulatively over the period of the bag immersion in water (Winkler et al., 2016), providing evidence of the dye tracer passage at that point. Five sampling points were selected to place the activated charcoal bags (Fig. 1c). For the duration of the experiment (from 16th July to 6th September 2021), two activated charcoal bags were placed at each sampling point. One activated charcoal remained throughout the experiment (captor C, 16th July – 6th September 2021) while the second (captor A, 16th July – 23rd July 2021) was replaced with another one (captor B, 23rd July – 2nd August 2021) on the day of the dye tracer injections (23rd July). The extraction was performed by placing 1 g of activated charcoal in 10 ml of a

5% solution of KOH in methanol. The resulting eluate was then injected into the measuring cell of the fluorometer for dye tracer detection.

Differently from the analysis of the activated charcoal bags, which allowed a qualitative interpretation, the field fluorometer enabled the quantification of the amount of dye tracer flowing at the downstream point (Fig. 1c). A GGUN-FL24 fluorometer was used, with a 5 min and 1 min recording rate in the week before injection (16^{th} – 23^{rd} July 2021) and after injection (23^{rd} July – 2^{nd} August 2021), respectively. The dye tracer recovery estimation was performed by integrating through time the measured concentration values multiplied by the discharge (Gaspar, 1987). The recovered mass of fluorescein was estimated from the fluorometer measurements using the QTRACER2 software that solves the equations from user-generated data input files through integration of consolidated hydraulic models (U.S. EPA, 2002). The recovered tracer concentration was estimated for the week following the injection, i.e., from 23^{rd} July to 2^{nd} August 2021. Only night data were considered (from 8pm to 6am) since a malfunction in the light radiation shield prevented the use of the complete data series.

3.4 Volumetric rock glacier variations

Measuring the actual contribution from permafrost ice melt to the water budget of rock glaciers has never been done (to the best of our knowledge) due to the extreme difficulties posed by the rock-glaciated environmental conditions. Here, the volumetric variations of the Gran Sometta Rock Glacier were used as a proxy for the interannual ice changes (cf., Halla et al., 2021). The surface changes (horizontal and vertical) were detected with unmanned aerial vehicle surveys on a yearly basis, around mid-August each year from 2018 to 2021 (Bearzot et al., 2022). The Structure-from-Motion technique (Westoby et al., 2012) was used to generate dense point clouds of the rock glacier area and to produce orthomosaics and Digital Surface Models (DSMs) through the Agisoft Metashape software (v. 1.5.5 and later versions) (further details in Supplement, Text S1 and Tab. S1). DSMs, orthomosaics generation, point clouds comparison, and systematic error assessment were analysed in Bearzot et al. (2022). After image alignment, all photogrammetric blocks (one for each year) were processed with the same parametrisation to keep constant the impact on the final outputs. Based on the multitemporal analysis of the annual DSMs, the annual volumetric changes were computed. The

mean, standard deviation (stdev), and residual errors of the elevation change rates were computed on stable areas outside the rock glacier, over the three time intervals (2018-2019, 2019-2020, and 2020-2021).

3.5 Chemical and isotopic analyses

To understand the chemical influence of the rock glacier discharge on the main stream, assess the hydrochemical differences between the two lobes, and disentangle the contribution of different water sources to catchment water, EC, pH, major ions (SO_4^{2-}, HCO_3^-, NO_3^-, Cl^-, PO_4^{3-}, NO_2^-, Ca^{2+}, Mg^{2+}, Na^+, K^+, NH_4^+), trace elements (Al, Ti, Cr, Mn, Mo, Co, Ni, Cu, Zn, As, Cd, Sn, Sb, Ba, Pb, Fe, V, Ag, Se, Hg), and water isotopes ($\delta^{18}O$, δ^2H, ^3H, $\delta^{13}C_{DIC}$) were analysed. Water samples for EC, pH, major ions, and trace elements were collected during three consecutive seasons, 2019-2020-2021 (June-July – October), approximately on a bi-weekly basis; water samples for isotopic analyses were collected only in 2021 (Fig. 1d). Samples were collected along the main stream, at sites *Up* and *Down*, and at the rock glacier springs, *White spring* and *Black spring*. Precipitation and snow samples were collected only for isotopic analyses, in 2021. For the precipitation, a collector was installed close to the Black lobe front and sampled at the same time of the chemical sampling (if precipitation occurred). One snow sample was collected on 9th July 2021 from a long-lasting snow patch; snowmelt water dripping from the snow patch was collected before interacting with the ground. Through the three-year period, 5 sampling surveys were performed in June-July, 8 in August, and 10 in September-October. Samples for $\delta^{18}O$ and δ^2H were collected at all sampling dates and sites, whereas selected dates and sites were chosen for ^3H and $\delta^{13}C_{DIC}$. An overview of the analysed parameters for each sampling date and site is reported in Tab. S2.

pH was measured using a GLP21 (Crison Instruments). Electrical conductivity (EC) at +20 °C was measured using a Metrohm 712 Conductometer. HCO_3^- was analysed with titration method. The concentrations of major ions were determined by ion chromatography, using a Dionex ICS1000 for cations and an Aquion for anions. Trace elements were determined by inductively coupled plasma-sector field mass spectrometry (Varian 720). Hg was determined using a DMA80 (Milestone). Analytical precision for major anions was < 10%, and for major cations and trace elements was < 5%. Charge balance error for each sample was always below 10%. Further information about the field sampling, sample treatment, and laboratory

analyses is reported in Supplement, Text S2, whereas the limit of detection (LOD) and quantification (LOQ) of each analyte are reported in Tab. S3.

$\delta^{18}O$ and $\delta^{2}H$ were analysed with a Cavity Ring Down Spectroscopy (Model L2130-I, Picarro). Isotopic composition was expressed as a δ (per mil) ratio of the sample to the Vienna Standard Mean Ocean Water (VSMOW), where δ is the ratio of $^{18}O/^{16}O$ and $^{1}H/^{2}H$. Analytical precision was 0.1 ‰ for $\delta^{18}O$ and 1 ‰ for $\delta^{2}H$. ^{3}H samples were analysed through Liquid Scintillation Counting (LSC), using Hidex 300SL, Tri-Carb-2500TR, andTri-Carb-3100TR. The ^{3}H LOD was 0.8 TU (tritium units). $\delta^{13}C_{DIC}$ (ratio of $^{12}C/^{13}C$ of dissolved inorganic carbon-DIC) was analysed through gas chromatography combustion isotope ratio mass spectrometry (GC-IRMS), using a GC-Isolink II IRMS system, Trace 1310, Conflow4 - IRMS Delta V Plus (Thermo Fisher Scientific). Analytical precision was < 0.5‰. Further details about the isotopic analyses and calibrations are reported in Supplement, Text S2. All isotopic analyses were performed by the IT2E Isotope Tracer Technologies Labs S.r.l.

To understand the influence of the rock glacier outflow on stream chemistry, differences among the sampling sites *Up*, *White spring*, *Black spring*, and *Down* were evaluated with the non-parametric one-way ANOVA (Kruskal-Wallis Test) using Wilcoxon scores, since several data series were non-normally distributed (Shapiro-Wilk Test) and/or variances were significantly uneven between groups (Levene's Test), even after data transformation. In addition, a simple two-component mixing-analysis was performed using EC, in order to assess the relative contribution of sites *Up* and RGs_{chem} (average values between *White spring* and *Black spring*) to *Down* (cf., Haag et al., 2000; Penna and van Meerveld, 2019). Findings of this last analysis are intended to further support the hydrological investigations.

A Principal Component Analysis (PCA), applying variable standardisation (scaling and centring), together with a correlation analysis (Spearman) were performed to visualise the differences in the relations among the water parameters characterising the springs at the two rock glacier lobes. In addition, based on the melt-out date of snow (obtained from the GST data elaboration), the variable “Days after snowmelt” was calculated for each sampling date, at the *White spring* and *Black spring* sites. This was used as a proxy to describe the seasonal patterns of water parameters while accounting for the contrasting end of the snowmelt period among different years (cf., Brighenti et al., 2021b).

All analyses were implemented in the R software (R Development Core Team, 2022), at a significance level of $p < 0.05$.

4. Results

4.1 Meteorological conditions and snow-cover duration

The meteorological conditions and the snow-cover duration during the investigated periods are shown in Fig. 2. To focus our analyses on the months that generally had positive air temperature and scares or absence snow cover, and to simplify the presentation of the data, only the meteorological and snow-cover characteristics from 1st June to 31st October were considered. The meteorological conditions during the investigated period were rather similar, although a moderately warmer mean air temperature was recorded in 2019 (+4.1 °C), with respect to 2020 (+2.5 °C) and 2021 (+2.6 °C). The cumulative liquid precipitation during the snow-free periods was 190 mm in 2019, 186 mm in 2020, and 189 mm in 2021. The fractional snow cover in the catchment, derived from remote sensing analysis, was less than 10% in mid-July and decreased to zero in late July-early August, with no relevant difference between the three investigated years (Fig. S1). The melt-out date of snow (obtained from the GST) occurred earlier in 2021 (25th June), with respect to 2019 (28th June) and 2020 (11th July).

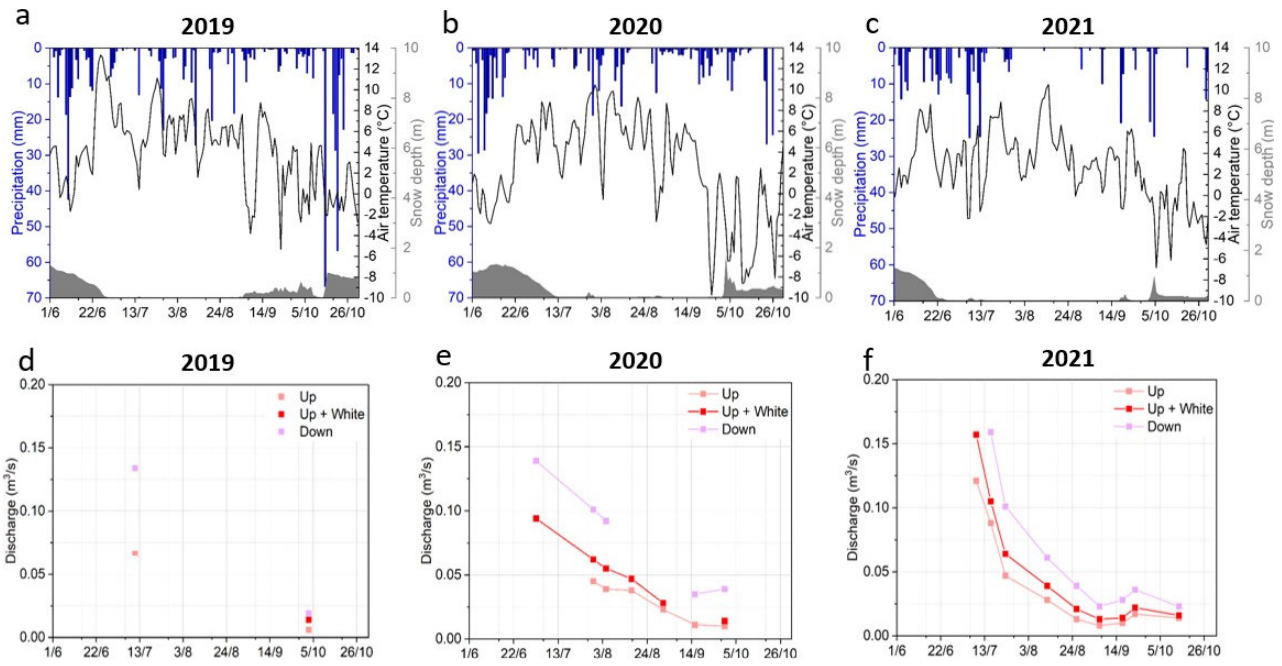

283

284 *Figure 2. Daily values of total precipitation (blue bars), air temperature (black line), and snow depth (grey area) in 2019 (a), 2020*
285 *(b), and 2021 (c) at the Cime Bianche AWS. Discharge rates estimated at the sites Up, Up+White, and Down in 2019 (d), 2020 (e) and*
286 *2021 (f). Data gaps in 2020 (e) are due to sensor malfunction.*

287

288 **4.2 Hydrological dynamics and water sources**

289 **4.2.1 Discharge patterns**

290 The results of the discharge measurements are shown in Fig. 2. In 2019, 2020, and 2021, the maximum
291 discharge rates occurred at *Down* site in July, with the highest value recorded in 2021 (0.16 $m^3 s^{-1}$). From July
292 onwards, discharges decreased at all three monitoring sites (*Up*, *Up+White*, and *Down*), to reach their
293 minimum values in September-October. The lowest value, 0.019 $m^3 s^{-1}$, was measured in October 2019 at site
294 *Up*.

295 Given the fact that the discharge measurements were discrete, single measurement values were aggregated
296 on a monthly basis (July, August, and September-October) in order to provide an overview of the seasonal
297 evolution of the rock glacier hydrological contribution to the Pousset stream over the entire research period.
298 The relative RGs_{hydro} contribution (composed of White + Black lobe contributions) to *Down* site showed a
299 gradual increase during the snow-free season, from 50% in July to 58% in August, finally peaking in
300 September-October at 63%; the overall relative hydrological contribution of RGs_{hydro} was 55% (Fig. 3a). The

Black lobe provided a higher relative contribution (71%), with respect to the White lobe, with rather stable values across the snow-free season (Fig. 3b).

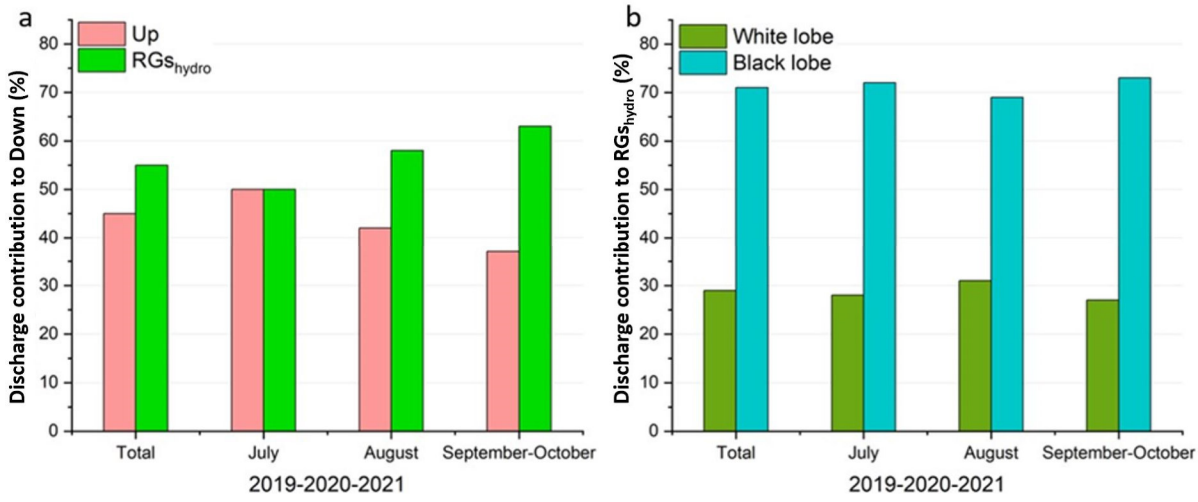

Figure 3. Total and monthly relative discharge contributions (%), over the entire research period (2019-2020-2021), of Up and RGs$_{hydro}$ (Black + White lobes) to the site Down (a) and of White and Black lobes to RGs$_{hydro}$ (b).

4.2.2 Response of the dye tracers

Fluorescein was tracked with a strong signal by two activated charcoal bags, while tynopal was not detected at any of the control points (Figs. 1c, S2). In the week following the injection (23rd July – 2nd August 2021, captors B), two activated charcoal bags detected the fluorescein at *Black spring* (n°3 in Fig. 1c) and *Down* (n°5 in Fig. 1c). This was confirmed by the analysis of the activated charcoal bags kept on site throughout the campaign, i.e., from 16th July to 6th September 2021 (captors C). These results also showed that there was no water exchange between White and Black lobes. In addition, since the activated charcoal bag on the left-hand orographic site of the Black lobe (n°4 in Fig. 1c) did not track fluorescein, it is reasonable to assume that this lobe does not release water laterally but only frontally, discharging directly (and only) into the Pousset stream.

During the sampling period, the field fluorometer at the site *Down* did not detect the transit of the tynopal tracer but only the fluorescein. Fluorescein arrival was detected 32 hours after the injection, although this transit time is likely overestimated since only night data were considered. In the week following the injection, a tracer recovery rate of 7.2% was estimated (3.6 g out of 50 g injected were recovered). The estimated mean tracer velocity was 3.4 m hour^{-1}.

4.2.3 Rock glacier volumetric variations

The negative and positive rock glacier surface elevation changes were predominantly related to the ridge and furrow topography. The highest amount of these variations matched with high horizontal displacements in the Black lobe toe. Conversely, smaller elevation changes occurred in the White lobe, where slower movements took place. The mean horizontal and vertical errors were within the order of –0.44 and 0.24 cm (stdev ranges 0.45–0.74) and between –3.00 and 9.44 cm (stdev ranges 7.84–12.61), respectively. The relative residual errors were 0.70, 0.76, and 0.71 cm for 2018–2019, 2019–2020, and 2020–2021, respectively. The uncertainty of image coregistration was also quantified along several profiles over the same stable terrain outside the rock glacier and the mean difference between the DSMs between –0.03 m and 0.03 m. Although these areas are considered stable, possible microtopography alteration could occur due to weathering and snow cover presence. The mean annual volumetric changes of the rock glacier surface were −70 mm yr^{-1}, −124.6 mm yr^{-1}, and −53.9 mm yr^{-1} in 2018−2019, 2019−2020, and 2020−2021 (Fig. 4), respectively. Since only two discharge measurements were performed in 2019, only the time intervals 2019−2020 and 2020−2021 were analysed in conjunction with rock glacier discharge rates (details in discussion).

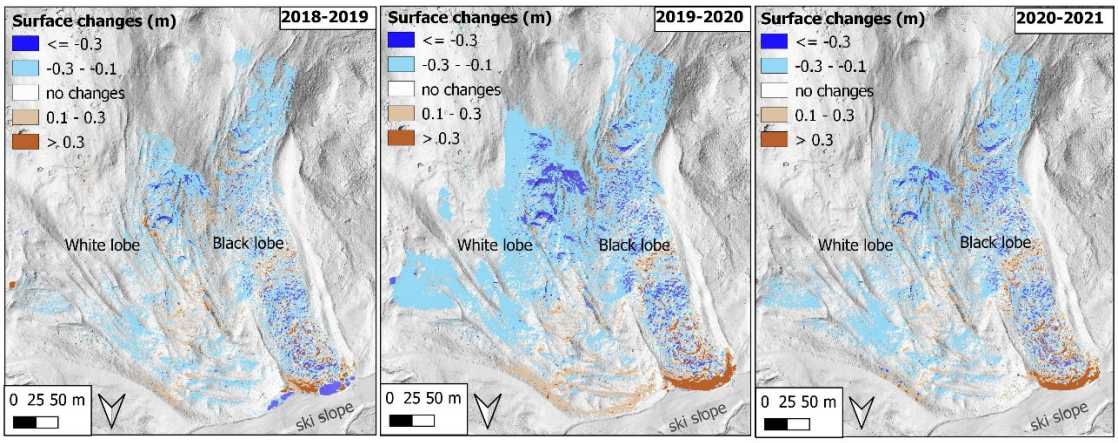

Figure 4. Surface vertical changes of the Gran Sometta rock glacier in 2018–2019, 2019–2020, and 2020–2021.

4.3 Thermal, chemical and isotopic characteristics of water

4.3.1 Water temperature

The mean daily water temperatures at sites *Up*, *Up+White*, *Black spring*, and *Down* are shown in Fig. S3. The *Black spring* temperature remained constant throughout the investigated period at +0.5±0.1 °C. This contributed to cooling down the Pousset stream; indeed, the mean temperature difference between *Down* and

344 *Up* sites was −2.2±1.0 °C. On average, the maximum temperature difference between *Down* and *Up* sites was
345 observed in August (−2.9±1.0 °C), while the minimum temperature difference was observed in October
346 (−1.0±0.3 °C). To investigate the cooling effect of the rock glacier springs, the relationship between the mean
347 daily water temperature difference between *Down* and *Up* and the mean daily air temperature was explored.
348 The results showed that a higher mean daily air temperature corresponded to a higher difference in water
349 temperature ($r = -0.71$, $p < 0.05$; Fig. 5).

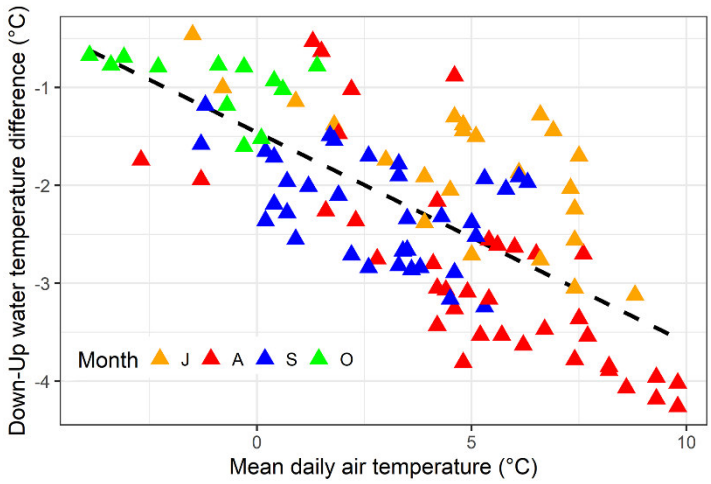

350

351 *Figure 5. Scatterplot between the mean daily air temperature (Cime Bianche AWS) and the mean daily water temperature difference*
352 *between Down and Up sites ($r = -0.71$, $p < 0.05$). Month: J = July, A = August, S = September, and O = October.*

353

354 The Black lobe caused the strongest cooling effect on the stream (difference between *Down* and *Up*: −2.2
355 °C; Fig. 5a), with *Up+White* and *Up* that were not significantly different, despite a decrease in stream water
356 temperature was also evident at *Up+White* site (difference between *Up+White* and *Up*: −0.8 °C; Fig. 6a). The
357 water temperature variance also decreased from *Up* to *Down*, both on seasonal (*Up*: 2.9±1.7 °C, *Down*: 0.9±1.0
358 °C) and daily bases (*Up*: 6.5±2.6 °C, *Down*: 2.5±1.6 °C), with the strongest thermal smoothing effect exerted
359 by the Black lobe (Fig. 6b).

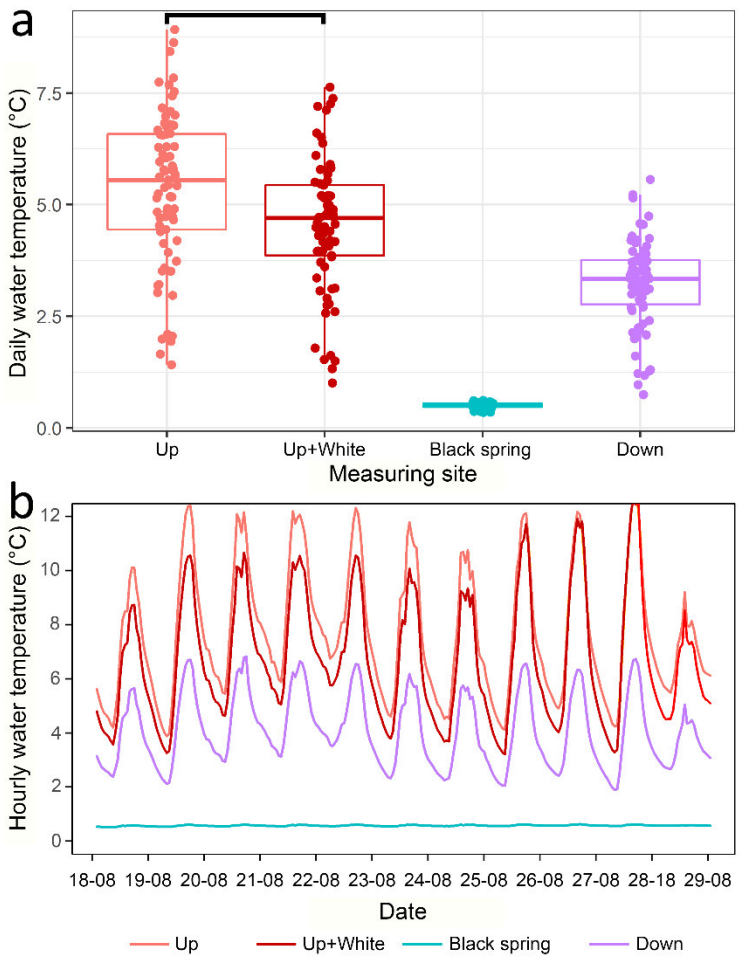

Figure 6. (*a) Boxplots (with jittered data points) showing the mean daily water temperature at the four measuring sites Up, Up+White, Black spring, and Down during all investigated period; the black segment indicates the sites that are not significantly different (p > 0.05). (b) Hourly water temperature at sites Up, Up+White, Black spring, and Down between 18th and 29th August 2020 (here taken as example).*

4.3.2 Water chemistry

A statistical summary of water chemistry for all sampling sites is reported in Tab. S4. On average, pH was basic (ca. 8) at all sampling sites. SO_4^{2-}, HCO_3^-, Ca^{2+}, and Mg^{2+} were the dominant ions. Ba was the only trace element consistently above LOQ for all samples, while all other trace elements were very close to or below LOQ and LOD for most of the analysed samples, thus they were excluded from further evaluation.

To understand the influence of the rock glacier on stream chemistry, the following parameters were selected: (i) EC, as an integrator of all dissolved ionic species; (ii) SO_4^{2-} and (iii) HCO_3^-, as dominant anions; (iv) Ca^{2+} and Mg^{2+}, as dominant cations, here considered together as Ca^{2+}+Mg^{2+} (expressed in μeq L^{-1}); (v) Ba; (vi) NO_3^- as an indicator of biotic processes (cf., Colombo et al., 2019; Williams et al., 2007). The

375 differences in the parameters previously indicated are shown in Fig. 7. All parameter values and concentrations
376 at *Down* site were significantly higher than at *Up*, except for HCO_3^-, which did not significantly differ among
377 all sites, according to Kruskal-Wallis Test with Wilcoxon scores. EC, SO_4^{2-}, and Ca^{2+}+Mg^{2+} were the highest
378 at *White spring* and *Black spring*, although not significantly different between them. Ba and NO_3^-
379 concentrations were the highest at *Black spring*. Considering EC as a tracer into a two-component mixing-
380 analysis, the relative contribution of the two lobes (RGs_{chem}) to *Down* increased from 49% in June-July to 62%
381 in September-October; the overall RGs_{chem} relative contribution was 55% (Fig. S4).

382 At the *Black spring* site, the first two axes of the PCA explained 77.7% of the total variance within the
383 dataset (Fig. 8a). The PC 1 was primarily a gradient of EC, major ions (except HCO_3^-), Ba, and, secondarily,
384 pH (which also influenced the PC 2). These variables were generally positively correlated with each other,
385 while pH was negatively correlated (Fig. 8b). Differently, HCO_3^- plotted along the PC 2 and it was not
386 correlated to any variable. In addition, the samples collected at *Black spring* in September-October plotted
387 almost exclusively on the right side of the first ordination, indicating that these dates were characterised by
388 higher EC, major ions (except for HCO_3^-) and Ba concentrations, and lower pH values, with respect to the
389 samples collected in June-July and August. At the *White spring* site, the first two axes of the PCA explained
390 69.8% of the total variance within the dataset (Fig. 8c). The main differences with respect to the PCA
391 performed at *Black spring* was that at *White spring* no evident seasonal variations emerged from the data and
392 correlations were generally weaker and even not significant (except for HCO_3^-) (Fig. 8d).

393 The differences in seasonal variations were further confirmed by looking at the trends of the main chemical
394 parameters (Fig. 9). Indeed, the *Black spring* exhibited evident increases in EC, major ions (except for HCO_3^-
395) and Ba values as a function of the days elapsed after the snowmelt period, while pH decreased, instead.
396 Differently, the *White spring* did not show significant seasonal trends, except for Mg^{2+}, which slightly
397 increased.

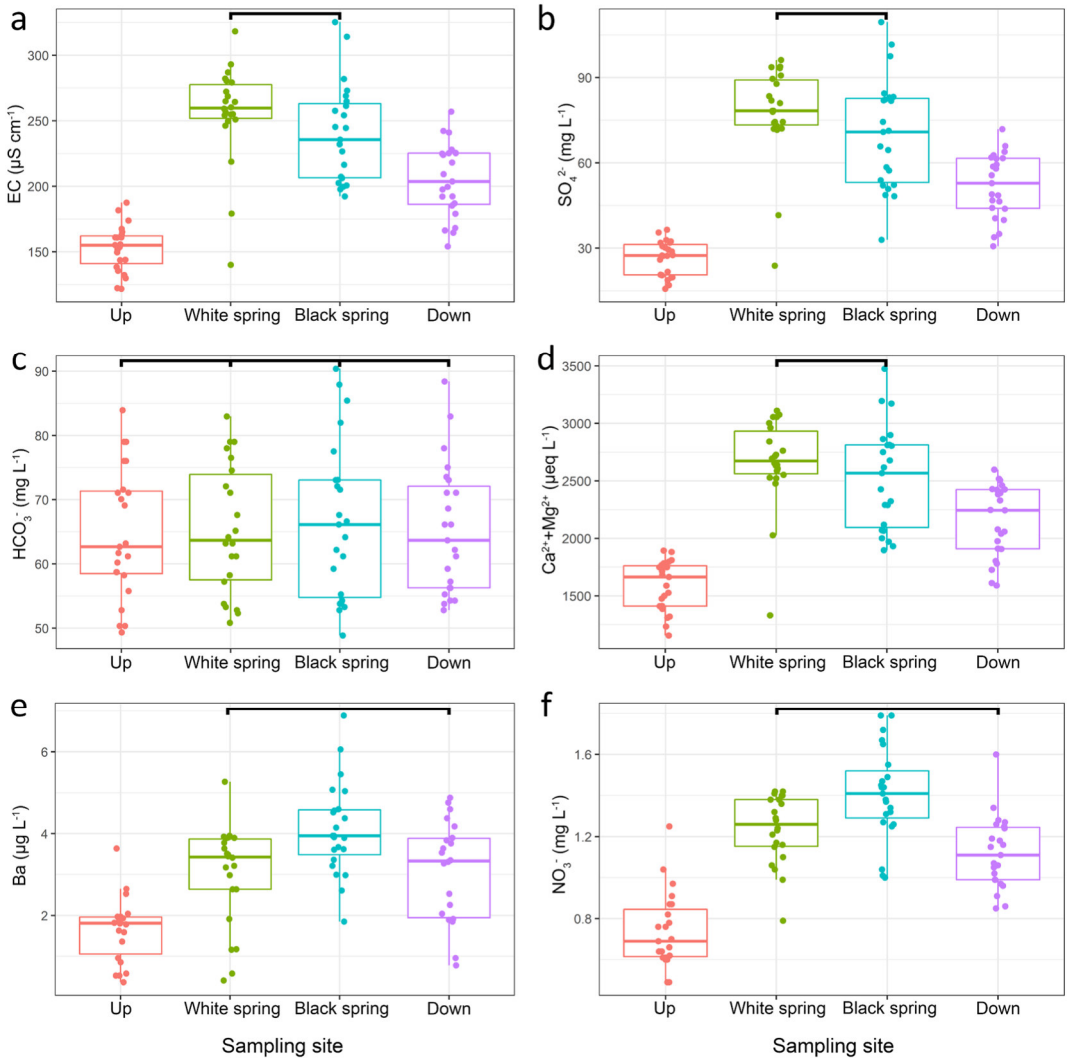

Figure 7. Boxplots (with jittered data points) showing the differences, at the four sampling sites Up, White spring, Black spring, and Down, among selected tracers: EC (a), SO_4^{2-} (b), HCO_3^- (c), $Ca^{2+}+Mg^{2+}$ (d), Ba (e), and NO_3^- (f). The black segments indicate the sites that are not significantly different ($p > 0.05$).

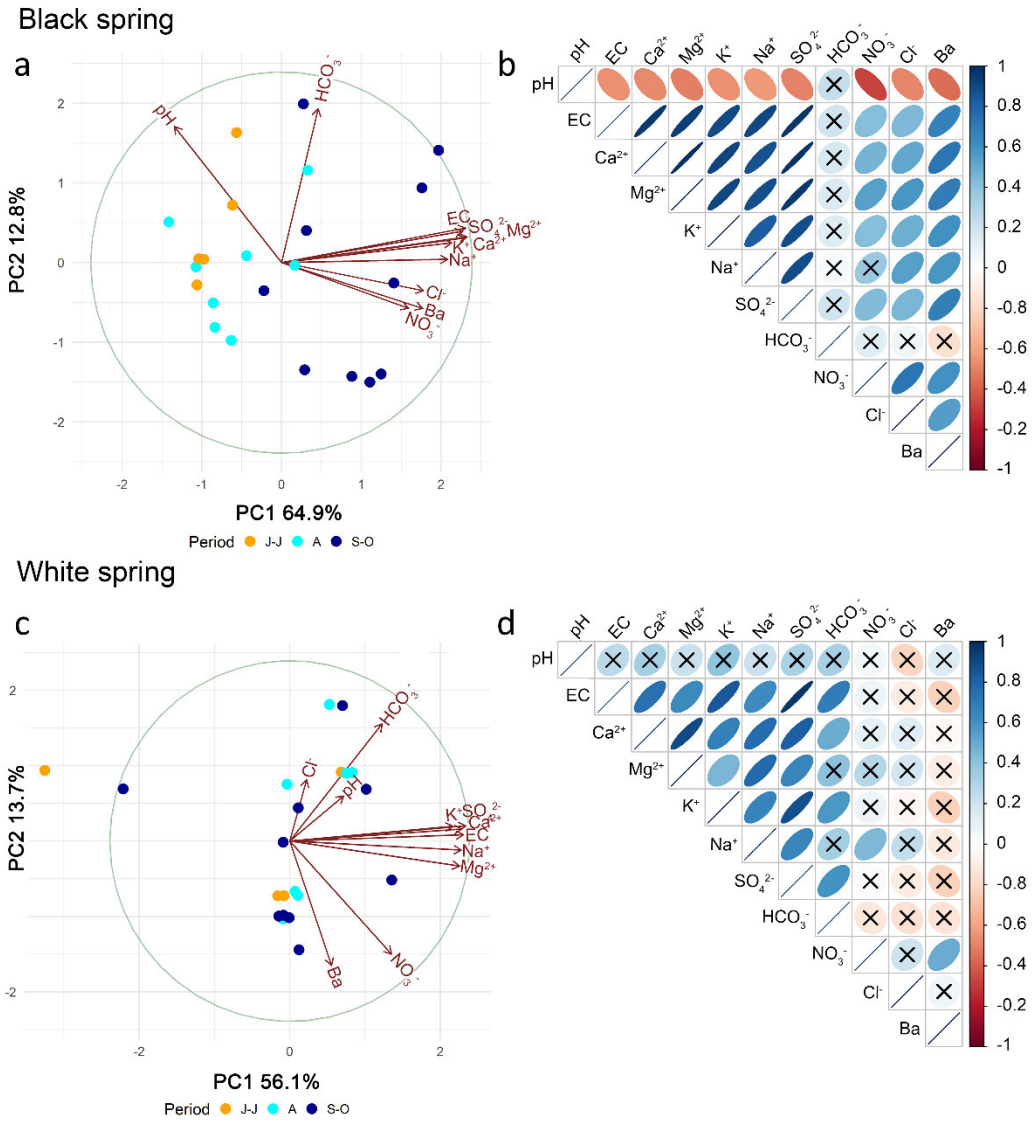

Figure 8. PCA plots and correlation matrices for Black spring (a and b) and White spring (c and d). In panels a and c, J-J = June-July, A = August, and S-O = September-October. In the correlation matrices in panels b and d, Spearman values are represented by different colours (blue = positive correlation, red = negative correlation) and ellipse orientation (left = negative correlation, right = positive correlations). Colour intensity and ellipse size represent the correlation strength (pale and wide = weak, intense, and narrow = strong). Crossed ellipses correspond to correlations that are not significant ($p > 0.05$).

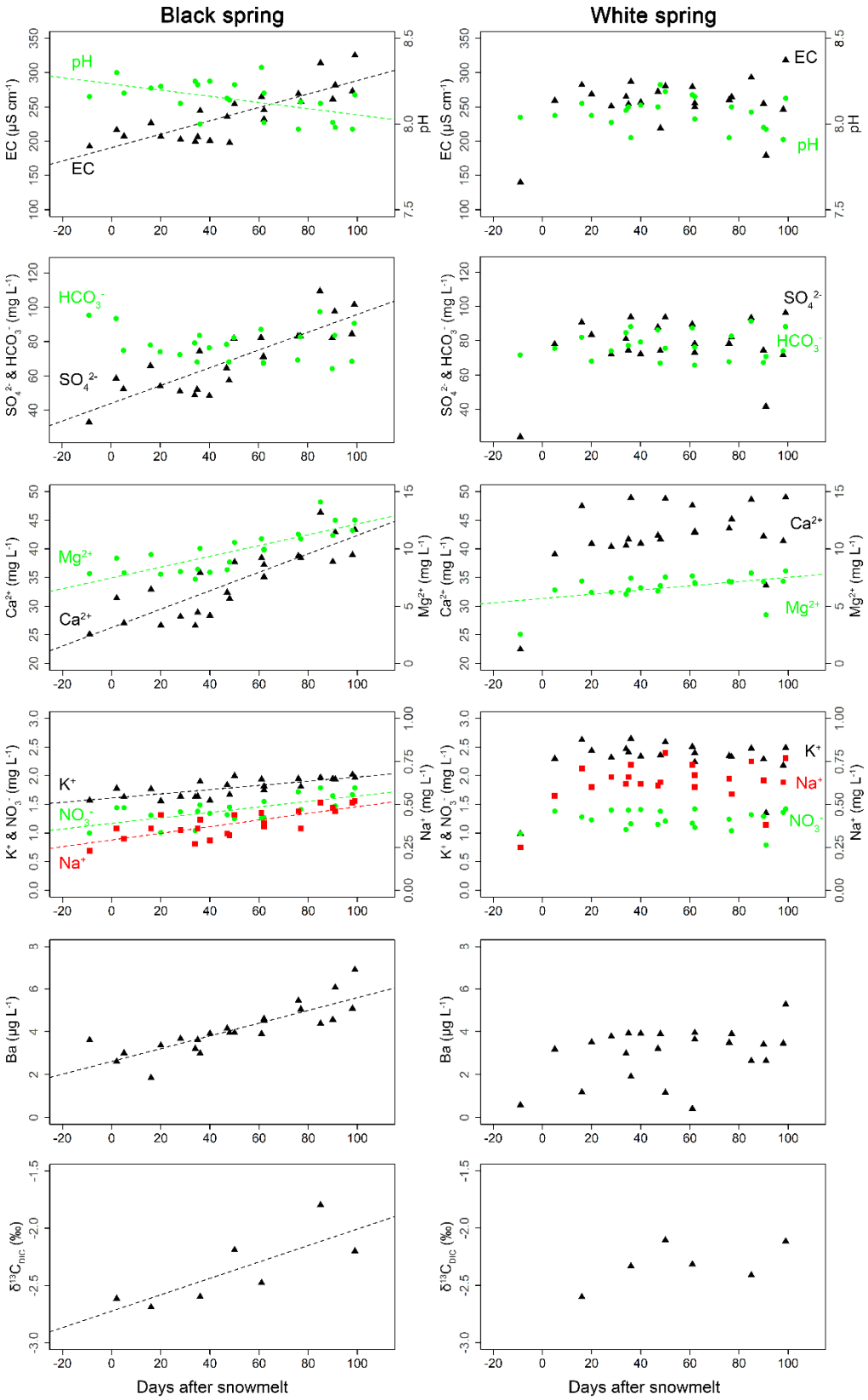

Figure 9. Seasonal trends of water parameters as a function of the days after the melt-out date of snow (derived from GST) at Black spring (left panels) and White spring (right panels). Interpolation lines represent significant linear regressions ($p < 0.05$).

4.3.3 Water and DIC isotopic signatures

The results of the isotopic analyses are presented in Tab. S4 and S5. *Precipitation* showed the most enriched values, with −9.1±0.7‰ for $\delta^{18}O$ and 59.5±4.3‰ for $\delta^{2}H$. On the opposite, the single sample for *Snow* evidenced the most depleted signal in the dataset, with values of −14.4‰ for $\delta^{18}O$ and −104.6‰ for $\delta^{2}H$. *Up* and *Down* sites together with *White spring* and *Black spring* signatures arranged in between *Precipitation* and *Snow*, with a variability between −13.5±0.3‰ (*White spring*) and −13.2±0.6‰ (*Up*) for $\delta^{18}O$, and between −93.6±2.2‰ (*White spring*) and −90.5±3.9‰ (*Up*) for $\delta^{2}H$. The stable water isotopic data are consistent with isotope compositions for the precipitation representative of the Northern Italian Meteoric Water Line (NIMWL) (Longinelli and Selmo, 2003; Fig. 10).

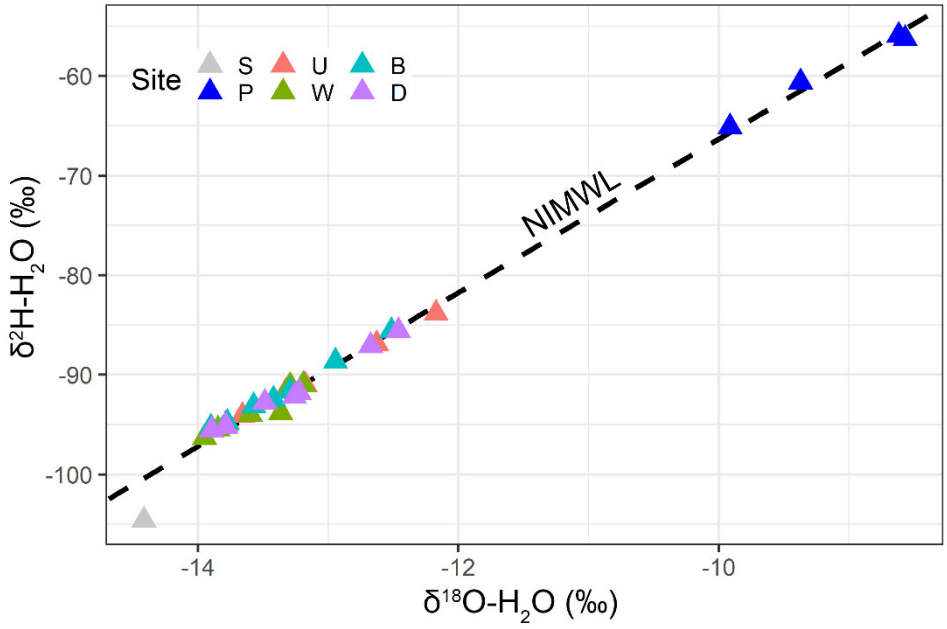

Figure 10. Dual-plot isotope distribution at the investigated sites, in 2021. Site: S = Snow, P = Precipitation, U = Up, W = White spring, B = Black spring, and D = Down. NIMWL: Northern Italian Meteoric Water Line.

Coupling chemistry and isotopes, it is possible to observe for the *Black spring* a strong positive correlation from July to October between $\delta^{18}O$ and SO_4^{2-} (here used as a tracer of weathering processes in cryospheric environment; cf. Colombo et al., 2019; Salerno et al., 2016), while just a slight increment for the *White spring* occurred (Fig. 11); by specifying this, the isotope "delta", expressed as the difference between the maximum and the minimum $\delta^{18}O$ measured was 1.39 and 0.76‰, for the *Black spring* and *White spring*, respectively. Even *Up* and *Down* sites recorded higher delta values than the *White spring* of 1.61 and 1.44‰, respectively.

From the dual-plot isotope distribution, it is possible to assert how signals related to the White lobe resulted more conservative than the ones of the Black lobe (Fig. 10), as the latter seemed to be more influenced by liquid precipitation.

Results for $\delta^{13}C_{DIC}$ ranged from −14.8 to −10.3‰ in *Precipitation*, while it was −11.7‰ in *Snow* (Tab. S5). $\delta^{13}C_{DIC}$ at *Up* site ranged from −5.6 to −4.5 ‰, while in rock glacier samples ranged from −2.7 to −1.8‰ (both found at *Black spring*). A significant trend toward a $\delta^{13}C_{DIC}$ enrichment over time was registered at the *Black spring,* whereas the *White spring* presented only a slight oscillatory behaviour during the investigated period (Fig. 9).

Data for ^{3}H were always above the LOQ (Tab. S5). Tritium content was measured in one July sample for *Snow* (6.8 TU), and a single sample collection was performed at *Up* (6.0 TU), *White spring* (4.7 TU), and *Precipitation* (6.0 TU), in September 2021. A prolonged monitoring of the *Black spring* revealed a slight variation in ^{3}H content, ranging between 4.8 (July and September 2021) and 7.0 TU (August 2021).

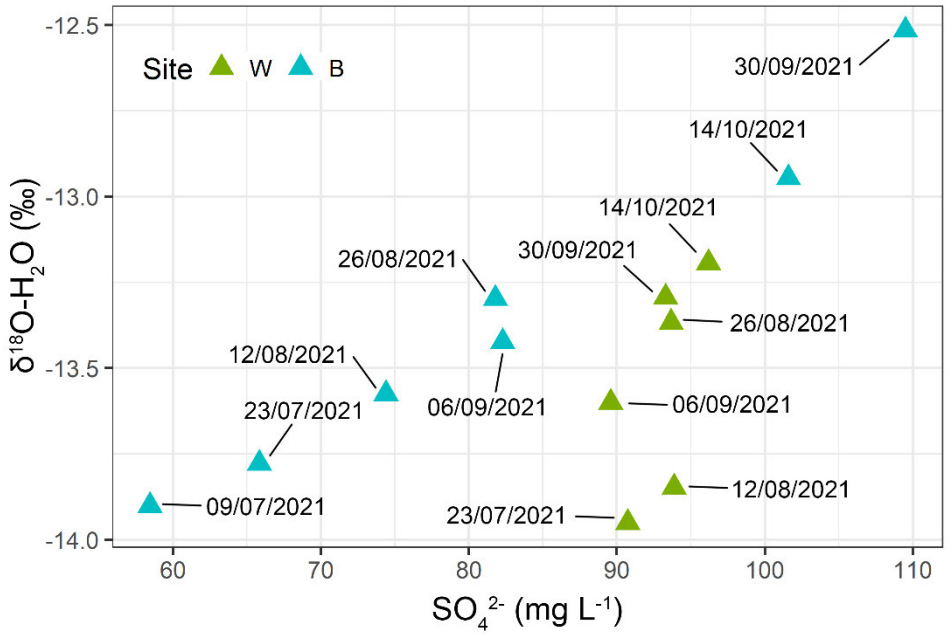

Figure 11. Scatterplot *between SO_4^{2-} and $\delta^{18}O$ at sites White spring (W) and Black spring (B), in 2021.*

5. Discussion

5.1 Hydrological dynamics and water sources

5.1.1 Rock glacier impact on hydrologic regime

449 The highest discharge rates at all measuring sites were measured at the end of the snowmelt period or right
450 after the melt out of snow (i.e., July). However, these were not the streamflow peaks, which likely occurred
451 during the peak snow-melt period in June (cf., Geiger et al., 2014; Krainer and Mostler, 2002), when our
452 measurement sites were inaccessible. With the progression of the snow-free season, discharge rates
453 significantly decreased, reaching their lowermost values in September-October, as observed in other high-
454 elevated and rock-glaciated settings (Harrington et al., 2018; Geiger et al., 2014; Krainer and Mostler, 2002).
455 The relative contribution of the rock glacier increased towards late summer - early autumn, with the highest
456 influence on the main stream measured in September-October (62-63%), as observed from both hydrological
457 and chemical measurements. Despite draining only 39% of the watershed area, the Gran Sometta Rock Glacier
458 contributed 55% of catchment streamflow during the period July – October. Therefore, our findings support
459 the concept of these landforms as important hydrogeomorphic units which can store and transmit quantities of
460 groundwater, modulating the catchment hydrologic response and sustaining the baseflow during the late
461 summer - early autumn (Wagner et al., 2021a; Harrington et al., 2018). Indeed, sediment accumulation and its
462 drainage processes in rock glaciers, together with the subsurface properties (e.g., porosity, transmissivity, and
463 storage capacity), can impact the seasonal streamflow (Hayashi, 2020; Harrington et al., 2018). In this sense,
464 rock glaciers have the net effect of increasing total surface runoff from alpine drainage basins, due to their
465 capability to act as impervious surfaces (Wagner et al., 2020; Harrington et al., 2018; Geiger et al. 2014),
466 playing a critical role as shallow groundwater reservoirs in mountain headwaters (Wagner et al., 2021a, 2020;
467 Hayashi, 2020; Winkler et al., 2018, Geiger et al., 2014).
468 During the period July – October, the Black lobe contributed significantly more (71%) than the White lobe
469 (29%) to catchment streamflow, with no relevant seasonal variations. It is known that different spatial
470 distribution, depth, and thickness of permafrost affect hydrology, infiltration, and runoff response in high-
471 mountain catchments (Rogger et al., 2017; Duguay et al., 2015; Geiger et al., 2014). Thus, it is possible that
472 the continuous layer of frozen ground (and ice) in the Black lobe resulted in larger hydrological contributions
473 (and possibly, runoff events) during the investigated snow-free seasons because of the more limited losses to
474 deep groundwater storage that, vice versa, could be enhanced in the White lobe (characterised by low content
475 and heterogeneous distribution of permafrost and ice) (cf., Rogger et al., 2017; Evans et al., 2015; Geiger et
476 al., 2014).

The dye tracer tests confirmed the diversity of water circulation in the two rock glacier lobes and therefore their hydrological behaviours. At the Black lobe, the fluorescein was tracked by both the activated charcoal bags and the field fluorometer, which showed the first detection of the tracer approx. 32 hours after the injection, with a recovery rate of 7.2% in the first week after the injection. The remaining percentage of dye infiltrated from the active layer and likely penetrated in the underlying zone. Thus, different flow paths might be present in the Black lobe: a shallower flow (on the surface of the permafrost table and above the ground ice) and intra- and sub-permafrost flows (cf., Jones et al., 2019; Winkler et al., 2016; Tenthorey, 1992). The tracer mass recovered is in line with what was found in other case studies dealing with rock glaciers (e.g., Mari et al., 2013).

Differently from the Black lobe, at the White lobe, the passage of the tracer (tynopal) was not tracked during the investigation period. Thus, this lobe could be characterised by the prevalence of a deeper, slow groundwater flow due to major areas of unfrozen layers responsible for groundwater storage and retarded runoff (Wagner et al., 2021b). In addition, in accordance with the geophysical data collected by Bearzot et al. (2022), the injection point of the tynopal was located in a thick unfrozen zone, therefore the dye tracer might have directly infiltrated to a great depth into the debris body and slowly circulated under the permafrost, thus further explaining a high residence time (cf., Rogger et al., 2017). Another reason for the non-detection of this tracer and for the lower discharge contribution may be related to the fracturing of bedrock and the presence of bedrock depression. Since this area was characterised by a small glacier during the Little Ice Age (Bearzot et al., 2022), it is also possible that glacier erosion created hummocks and depressions in the bedrock of the watershed (Harrington et al., 2018). The fractured rocks might allow the tynopal and water for a slow drainage of groundwater stored in partially filled depressions through bedrock fractures and, as a consequence, potentially drain part of the tynopal/water outside the investigated watershed. On one hand, this last case would imply that the difference in the discharge between the two lobes may not be solely due to internal hydrological systems driven by different cryospheric conditions, although their contrasting hydrochemical patterns indicate a relevant role of permafrost and ice distribution in the two lobes (details in 5.2.2). On the other hand, this would imply an underestimation of the potential water resource that could be provided by our rock glacier, thus further highlighting its relevant role as groundwater reservoir.

505 **5.1.2 Water sources and estimated contribution from internal ice melt**

506 The distinction of different water sources composing rock glacier outflows is generally based on qualitative
507 or indirect approaches rather than built on reliable measurements of individual system components combined
508 with quantitative measurements. Here, different lines of evidence have been used to trying dealing with this
509 issue.

510 The two lobes showed similar $\delta^{18}O$ and $\delta^{2}H$ isotopic compositions, also similar to stream water, thus ruling
511 out the hypothesis of relevant, different recharge inputs within the investigated systems. The isotopic
512 composition of rock glacier outflows generally represents the reflection of a mixture of at least three
513 components with different contributions over the hydrological year. In addition to precipitation and snow
514 contributions, the third component corresponds to the groundwater baseflow input plus ice melt, whose
515 isotopic fingerprint is not always easy to assess (Hayashi, 2020; Sileo at al., 2020). Differently, a higher
516 variability in water stable isotopes was found at the Black lobe, as an indication of a system more prone to a
517 local recharge influence and/or just likely more connected to the subsurface. The significant shift in the Black
518 lobe stable isotope values reflected a seasonal pattern in accordance with concentration data interpretation,
519 evidencing a more hydrologically responsive system (i.e., faster water circulation). A more conservative
520 flowpath might describe the White lobe behaviour (i.e., slower water circulation). Therefore, stable water
521 isotopes confirmed the existence of different internal hydrological systems in the two lobes, although pointing
522 to similar recharge sources (also in the stream), thus suggesting minor ice melt inputs from both lobes,
523 assuming ice melt having a well-distinguishable isotopic signature (cf., Williams et al., 2006).

524 Considering ^{3}H, it represents a valuable qualitative tracer due to spike of atmospheric ^{3}H in fallout from
525 bomb testing in the 1950s (Celle-Jeanton et al., 2002). ^{3}H has a half-life of 12.4 years, such that precipitation
526 before the 1950s will contain less than 0.1 TU, whereas precipitation that fell during the decade of 1950–1960
527 will now contain approximately 70 TU (Celle-Jeanton et al., 2002). Tritium is suitable for untangling residence
528 times for young flowpaths (in a geological understanding), being the ideal tracer for approx. 80-year-old water
529 systems (Kralik, 2015). Tritium data for *Precipitation* and *Snow* reflected the signal of modern precipitation
530 monitored in central Europe (WISER, https://nucleus.iaea.org/wiser). Only a slight depletion in ^{3}H content
531 was observed for stream and rock glacier springs, if compared to precipitation data, suggesting a relatively
532 modern water (infiltrated after the ^{3}H peak). Considering the September 2021 sampling, when the contribution

of ice melt should have been at its maximum, ^{3}H values in the rock glacier springs and the stream differed only by a maximum of 1.3 TU, possibly indicating a slight difference in residence time (≤ 1–2 years, c.f., Munroe, 2018). Thus, a relevant hydrological contribution to the rock glacier discharge from the melting of old permafrost ice (with age from centuries to millennia?) and/or transitional-layer ice at the top of permafrost (decades old?) was unlikely. It is also true that the seasonal (annual) active-layer ice (i.e., the superimposed ice that forms each spring due to the refreezing of part of percolating melt water) might have contributed to the rock glacier discharge. However, the lack of sensitivity in discretizing such small differences in residence time represents a limitation of the qualitative method using solely ^{3}H data. For further discussion aimed at a fine interpretation of the ice melt apparent ages (Suckow, 2014), ^{3}H data needs to be coupled with information of the dissolved ^{3}He generated from ^{3}H decay (Schlosser et al., 1988; Solomon et al., 1995), which is still poorly documented for alpine catchments (e.g., Munroe, 2018).

Based on the rock glacier discharge rates and volumetric variations, the overall ice melt contribution was estimated to represent less than 3.5% of the rock glacier discharge (3.3% in 2019−2020 and 2.5% in 2020−2021). Estimation of ice melt contribution was not performed for the time-lapse 2018−2019; however, taking into account that the volumetric variation in 2018−2019 (−70 mm yr^{-1}) fell within the range measured for 2019−2020 and 2020−2021 (−53.9 ÷ −124.6 mm yr^{-1}), ice melt contribution in 2018−2019 did not likely diverge consistently from the presented estimations. Even assuming all ice melt occurring in September-October, when active layer depth is usually at its maximum, the net contribution of permafrost ice melt in the baseflow period would be 7% and 10% for 2019−2020 and 2020−2021, respectively. It is worth noting, though, that these values are surely overestimated since they refer to both ice and sediment losses. In this regard, due to its advancing movement, the rock glacier front is cut every year and the material removed to allow the ski slope (in winter) and the service road (in summer) to be opened (Bearzot et al., 2022).

In light of these findings, internal ice melt should be considered a minor contributor to the rock glacier discharge, as already reported in other rock-glaciated settings (Harrington et al., 2018; Krainer et al., 2015).

5.2 Thermal and chemical influence on stream water

5.2.1 Water temperature

560 The low water temperature of the Black lobe spring, near 0 °C, suggests that the water flow was in direct
561 contact with ice or permafrost within the debris deposit (Scapozza et al., 2019; Millar et al., 2013). The rock
562 glacier discharge lowered the average water temperature of the main stream by ca. 2.2 °C, on average. The
563 thermal effect of the rock glacier was greatest in August, when the thermal effect of the rock glacier was
564 strongest (mean: 2.9 °C; daily maximum: 4.3 °C). However, the cooling effect of the rock glacier decreased
565 during periods with lower air temperature (and diminished solar radiation) and higher influence of snowmelt
566 (e.g., early July and October), which caused upstream temperature to decrease. Our findings are in agreement
567 with Harrington et al. (2017), who found a rock glacier spring to exert a dominant control on stream
568 temperature during the summer months, regardless of the magnitude of the distributed energy fluxes.
569 The thermal influence of the two lobes also acted on the amplitude of the daily thermal variations in the
570 main stream, greatly reducing them downstream. The thermal variations are generally reduced in the outflows
571 of rock glaciers, due to the water flowing in direct contact with ice or permafrost body (Colombo et al., 2018c;
572 Carturan et al., 2016; Millar et al., 2013; Krainer et al., 2007) and the "thermal smoothing effect" of the coarse
573 debris cover (Harrington et al., 2017; Winkler et al., 2016).
574
575 **5.2.2. Water chemistry**
576 The influence of the rock glacier on the main stream was also evident from a purely chemical standpoint.
577 Indeed, most of the solutes displayed higher concentrations at the *Down* site (after the water input from both
578 lobes) with respect to the *Up* site. Rock glaciers are known to act as a solute-concentrating mechanism
579 (Brighenti et al., 2019; Colombo et al., 2018c) increasing, in their waters, the concentrations of several
580 weathering products (e.g., SO_4^{2-}, Ca^{2+}, Mg^{2+}) (Colombo et al., 2018b). This is commonly attributed to the
581 enhanced water-rock contact, together with thawing of permafrost and the release of solute-enriched icemelt
582 (Colombo et al., 2018b; Munroe, 2018; Williams et al., 2006).
583 Among the different solutes, SO_4^{2-} have been often found to be particularly concentrated in rock glacier
584 waters (Steingruber et al., 2020; Rogora et al., 2020; Ilyashuk et al., 2018; Williams et al., 2006). In our case,
585 much higher (up to three times) mean SO_4^{2-} concentrations were found at the lobes with respect to *Up* site,
586 while no HCO_3^- enrichment was found in the rock glacier water. $\delta^{13}C_{DIC}$ showed enriched values at the rock
587 glacier lobes (mean: −2.3‰) with respect to stream water (mean: −5.1‰) (further details about the $\delta^{13}C_{DIC}$

dynamics are reported in the Supplement, Text S3). This evidence seems to indicate a similar carbon source, although with a higher contribution from carbonate weathering by sulphuric acid (e.g., produced by sulphide oxidation) in the rock glacier (cf., Ulloa-Cedamanos et al., 2021; Spence and Telmer, 2005). The S-ratio (SO_4^{2-} /(SO_4^{2-}+HCO_3^-), where units of concentrations are expressed in μeq L^{-1}; Tranter et al., 1997) and the R_{SO4} (the molar ratio SO_4^{2-}/(Ca^{2+}+Mg^{2+}); Ulloa-Cedamanos et al., 2021) were 0.58 at the rock glacier and 0.34 at *Up*, on average. S-ratio and R_{SO4} equal to 0.5 correspond to predominating carbonate weathering by sulphuric acid, while carbonate weathering by carbonic acid decreases both indices below 0.5 due to excess of HCO_3^-. S-ratio and R_{SO4} values above 0.5 at the rock glacier indicate a SO_4^{2-} excess; a combination of sulphide oxidation and gypsum dissolution might be responsible for this occurrence (cf., Ulloa-Cedamanos et al., 2021; Cooper et al., 2002). Even though there are no mapped gypsum deposits within the catchment nor were found during targeted field surveys, they might be present in the sub-surface in association with dolomites. Alternatively, the weathering of calcium silicates driven by sulphide oxidation might also contribute in causing the SO_4^{2-} excess, although considering the predominant presence of carbonatic rocks with no high silica content and the very low contribution of Na^+ and K^+ to the cations at all sampling sites (always ≤ 3%, on average), this process should not be relevant (cf., Steingruber et al., 2020; Spence and Telmer, 2005). However, further analyses are necessary to distinguish between specific weathering processes and discriminating between different geo-lithological sources, such as detailed lithological investigations and additional geochemical analyses (e.g., sulphur and oxygen isotopes of sulphate as well as calcium and magnesium isotopes; e.g., Steingruber et al., 2020; Colombo et al., 2018b). Nevertheless, our findings are in agreement with previous studies which attributed the enhanced release of SO_4^{2-} from rock glaciers to different weathering processes (and their combination) in an environment with high availability of fresh mineral surfaces and moisture together with the presence of sulphide-bearing minerals (e.g., pyrite) and/or gypsum (Rogora et al., 2020; Steingruber et al., 2020; Ilyashuk et al., 2018; Williams et al., 2006).

Regarding the generally low concentrations of trace elements, they can be explained by the relevant presence of carbonate rocks and basic pH (cf., Colombo et al., 2019). Previous studies reported high trace element concentrations in rock glacier meltwaters, although generally associated with acid or ultrabasic metamorphic lithologies (Colombo et al., 2019; Ilyashuk et al., 2018; 2014; Thies et al., 2013). In our case,

only Ba was consistently above LOQ, showing an enrichment in the rock glacier outflows and downstream along the main stream.

NO_3^- concentration was also higher at the lobes. This could be attributed to the presence of soils and vegetation in restricted areas along the main stream, with the biological community playing a relevant role in limiting losses of NO_3^- to the stream (cf., Colombo et al., 2019; Balestrini et al., 2013; Kopácek et al., 2004), and/or to microbial communities adapted to the extreme environment of the rock glacier as potential sources of nitrate in its outflow (Williams et al., 2007).

Evident differences in the seasonal trends of solutes, as a function of the days elapsed after the seasonal snow cover disappearance, were noted in the two lobes. Seasonal increases in solute concentrations are usually attributed to the progressive reduction of solute-diluted snowmelt (early summer) (e.g., Engel et al., 2019) and to increasing contributions of solute-enriched water fluxes when the active layer thickness is at its maximum (late summer - early autumn; Brighenti et al., 2021b; Colombo et al., 2019; 2018b; Williams et al., 2006). Considering that the two lobes are adjacent and thus have similar snowmelt duration, one would expect comparable hydrochemical behaviours. However, this was not the case. Thus, it is possible that different flowpaths, as deduced by the hydrological analyses, corresponded also to different solute sources into the two lobes. Indeed, besides the absolute variations in solute concentrations, different proxies indicated possible seasonal changes in the weathering processes in the Black lobe (which were not observed at the White lobe). Mean S-ratio and R_{SO4} values increased from June-July (S-ratio: 0.48; R_{SO4}: 0.51) to September-October (S-ratio: 0.63; R_{SO4}: 0.61). In addition, $\delta^{13}C_{DIC}$ showed a seasonal enrichment with a range from –2.7 to –1.8‰ and R_{SO4} and $\delta^{13}C_{DIC}$ exhibited a significant correlation ($r = 0.82$, $p < 0.05$). Finally, pH seasonally decreased. These patterns point towards seasonal, relative increasing contributions from weathering processes associated with sulphide oxidation (Ulloa-Cedamanos et al., 2021; Colombo et al., 2019; Williams et al., 2006). This occurrence might indicate that, in the Black lobe, where permafrost and ice content is higher (with possible greater moisture content), seasonal active layer thickening, thawing of permafrost, and melting of ice would progressively open flowpaths in the lobe interior (percolation of near-surface water into rock-ice matrix might also occur). Then, increasing chemical fluxes would originate from chemical weathering of freshly exposed mineral surfaces (further enhanced by the decreasing water flow velocity through the rock glacier system over the course of the summer) and, secondarily, from solute-enriched icemelt (cf., Colombo et al., 2018c; Williams

et al., 2006). Differently, in the White lobe, this change in space and time of flowpaths, causing seasonal changes in chemical weathering dynamics, would be reduced, given the lower permafrost and ice content and the possible presence of preferential flowpaths thorough unfrozen zones in the lobe interior. Lower shear stress and friction in the White lobe (characterised by slower displacement rates with respect to the Black lobe) might also play a role in lowering the production of fresh mineral surfaces inside the lobe.

5.3 Environmental implications

Due to climatically-driven glacial recession, glacier melt contribution to streamflow will gradually decline whereas runoff from rock glaciers will become more relevant, due to their water storage capability and longer response times to climatic changes (Wagner et al., 2021a; Jones et al., 2019). However, based on our observations and most recent findings, only a minor component of the water storage capability of rock glaciers, directly contributing to runoff, could be represented by melting ice. This is due to the slow conduction of heat through the ground, causing internal ice to melt at slow rates (Arenson et al., 2022). In addition, unlike solid water storage resources, such as glaciers and snow, the replenishable storage volume of rock glaciers is expected to increase as the degradation of permafrost (and ice melting) proceeds (Hayashi, 2020; Jones et al., 2019). Thus, rock glaciers will be an important source of water supply for both sensitive ecosystems and human consumption in the future, even with reduced hydrological fluxes originating from ice melt (Wagner et al., 2021a; Hayashi, 2020; Winkler et al., 2016).

Rock glaciers could play an increasingly relevant role not only by influencing timing and magnitude of runoff, but also its thermal conditions. Water temperature in mountain streams is highly sensitive to atmospheric warming (Michel et al., 2022; van Vliet et al., 2013), representing a critical factor for aquatic ecosystems (Niedrist and Füreder, 2020). The thermal state of streams in mountainous areas is expected to become even more vulnerable to warming in the near future due to the expected reductions in snow and glacier-melt inputs (Michel et al., 2020). Rock glaciers could compensate for air temperature warming trends and lower contributions of meltwater from snow and glaciers in mountain streams, especially during warm atmospheric periods. This effect could persist even after most of the ice will have melted, since low water temperatures have been measured in springs emanating from rock glaciers with low (Harrington et al., 2017)

to no ice content (Winkler et al., 2016), due to the physical characteristics of the coarse blocky cover (Harrington et al., 2017; Winkler et al., 2016).

The hydrological and thermal role of rock glaciers could be accompanied by a chemical influence. Under continued atmospheric warming, a sustained glacier recession in combination with a prolonged snow-free period may further boost the hydrochemical influence of intact rock glacier outflows. This influence will be more evident during baseflow conditions, in late summer - early autumn, when the relative hydrological contribution of rock glaciers is higher, with potentially significant effects on surface-water ecology and for drinking water quality (Brighenti et al., 2019; Colombo et al., 2018b; Ilyashuk et al., 2018; 2014; Thies et al., 2018).

5.4 Research limitations

The main limitations of our approach are related to groundwater circulation and discharge analyses. Indeed, the dye tracer investigation was performed only for a relatively short amount of time during the snow-free season, therefore no information on the hydrological behaviour of the lobes was obtained for the snow-covered season. For this reason, the groundwater circulation investigation left some open considerations. For instance, the residence time of the dye tracer into the White lobe is unknown since the tynopal was not tracked during the campaign months in 2021, and further observations were not performed during the following melt season(s). Thus, the White lobe may contribute more groundwater, with respect to the Black lobe, especially during the snow-covered season, due to its internal characteristics, hence potentially representing an underestimated water source when considering the entire hydrological year. In addition, the possible presence of depressions and fractures in the bedrock would require additional investigations in other downstream springs and water bodies, potentially revealing different flow paths. Furthermore, although the seasonal variations in the relative contribution from the rock glacier agree well with the chemical analysis, thus confirming the goodness of our findings, they were not investigated continuously. Therefore, our understanding of the rock glacier hydrological behaviour is partial. For instance, the discharge response to precipitation events is unknown, and this could have been helpful in drawing a clearer picture of the internal hydrological systems of the two lobes. Finally, in the *Up* catchment, small rock glaciers, protalus ramparts, and ice-cored moraines are potentially present (as deduced from aerial and satellite images), even though targeted geomorphological

surveys have not been performed so far. These landforms share similar sedimentological features with the analysed rock glaciers; thus, it is possible to assume the existence of non-negligible hydrological contributions from these deposits, especially during the baseflow period. This occurrence would imply that, in other rock-glaciated catchments without these landforms, the hydrological relevance of rock glaciers might be higher than what estimated in this study.

Further uncertainties exist on the potential impacts of the rock glacier influence on the thermal and chemical conditions of the main stream, chiefly involving their propagation downstream, which was not investigated in our study. For instance, atmospheric conditions are the primary driver of the energy budget in mountain streams, with a dominant role of air temperature and radiation (Somers et al., 2016; Khamis et al., 2015; Magnusson et al., 2012). Therefore, a rather rapid equilibration of water temperature downstream might occur. However, the cooling effect of rock glacier discharge has been found to persist over several hundreds of metres, highlighting an overarching role of the large (negative) advective heat flux of the cold rock glacier discharge on stream energy fluxes (Harrington et al., 2017). Similarly, rock glacier discharge has been found to exert a significant influence on the downstream hydrochemistry of alpine streams, up to 3 km, highlighting its importance on the alpine river networks (Brighenti et al., 2019).

6. Conclusions

This study investigated the hydrological, thermal and chemical influence of an intact rock glacier on a high-elevation stream. Despite the estimated minor contribution from ice melt, the rock glacier springs sourced a disproportionately large amount of discharge to the main stream during the investigated snow-free seasons, with increasing contribution towards late summer and early autumn. This occurrence confirms the importance of rock glaciers as water sources, especially in those periods when the contribution of snowmelt is reduced or absent. In addition, the cold-water discharge from the rock glacier significantly cooled down the stream water temperature, with a larger influence during warm atmospheric periods. The chemical characteristics of the main stream were also impacted by the rock glacier discharge. Indeed, solute-concentrated waters sourcing from the rock glacier significantly increased the concentrations of most solutes in the stream. Remarkably, the two lobes forming the rock glacier, characterised by different permafrost and ice content, displayed evident contrasting hydrological and chemical behaviours. Thus, despite both lobes being intact and active, different

internal hydrological systems, likely driven by different cryospheric conditions, seemed to play a relevant role in shaping their hydrological and chemical response.

In the future, the increasing relevance of rock glaciers as water resources could be accompanied by an increasing chemical influence, with potentially significant effects on surface-water ecology and drinking water quality. At the same time, rock glaciers could play a role as thermal buffers on mountain streams, considering air temperature warming trends and lower contributions of water from melting snow and glaciers. Future work should focus on long-term hydrological and hydrochemical monitoring of rock glacier discharge and affected surface waters, assessing the downstream propagation of this "rock glacier effect".

Acknowledgements

This research was funded by the Italian MIUR project Dipartimenti di Eccellenza (2018-2020) and by the Interreg V-A IT-CH 2014-2020 project Reservaqua. Nicola Colombo and Michele Freppaz were partially supported by the project NODES, which has received funding from the MUR-M4C2 1.5 of PNRR with grant agreement no. ECS00000036. We would like to thank Andrea Benech, Michela Alessio, Michel Isabellon, Paolo Proment, and Roberto Garzonio for their help in data acquisition and analysis.

Reference list

Arenson, L.U., Harrington, J.S., Koenig, C.E.M., et al., 2022. Mountain permafrost hydrology – a practical review following studies from the Andes. Geosciences, 2022, 12, 48. https://doi.org/10.3390/geosciences12020048.

Balestrini, R., Arese, C., Freppaz, M., et al., 2013. Catchment features controlling nitrogen dynamics in running waters above the tree line (central Italian Alps). Hydrol. Earth Syst. Sci., 17, 989–1001.https://doi.org/10.5194/hess-17-989-2013.

Bearzot, F., Garzonio, R., Di Mauro, B., et al., 2022. Kinematics of an Alpine rock glaciers from multi-temporal UAV surveys and GNSS data. Geomorphology, 2022. Doi: 10.1016/j.geomorph.2022.108116.

Brighenti, S., Hotaling, S., Finn, D.S., et al., 2021a. Rock glaciers and related cold rocky landforms: overlooked climate refugia for mountain biodiversity. Glob. Change Biol., 1-14. Doi: 10.1111/gcb.15510.

753 Brighenti, S., Tolotti, M., Bruno, M.C., et al., 2021b. Contrasting physical and chemical conditions of two
754 rock glacier springs. Hydrological Processes, 35: e14159. https://doi.org/10.1002/hyp.14159.
755 Brighenti, S., Tolotti, M., Bruno, M.C., et al., 2019. After the peak water: The increasing influence of rock
756 glaciers on alpine river system. Hydrological Processes, 33(21), 1-20. https://doi.org/10.1002/hyp.13533.
757 Carturan, L., Zuecco, G., Seppi, R., et al., 2016. Catchment-scale permafrost mapping using spring water
758 characteristics. Permafrost and Periglacial Processes, 27, 253-270. Doi: 10.1002/ppp.1875.
759 Celle-Jeanton, H., Gourcy, L., Aggarwal, P., 2002. Reconstruction of tritium time series in precipitation. In:
760 Study of Environmental Change Using Isotope Techniques International Conference, 2001 April 23–27,
761 Vienna. IAEA in Austria, IAEA-CN-80/11P.
762 Colombo, N., Salerno, F., Martin, M., et al., 2019. Influence of permafrost, rock and ice glaciers on chemistry
763 of high.elevation ponds (NW Italian Alps). https://doi.org/10.1016/j.scitotenv.2019.06.233.
764 Colombo, N., Sambuelli, L., Comina, C., et al., 2018a. Mechanisms linking active rock glaciers and impounded
765 surface water formation in high-mountain areas. Earth Surface Processes and Landforms, 43(2), 417-431.
766 https://doi.org/10.1002/esp.4257.
767 Colombo, N, Salerno, F., Gruber, S., et al., 2018b. Impacts of permafrost degradation on inorganic chemistry
768 of surface fresh water. Global and Planetary Change, 162, 69-83.
769 https://doi.org/10.1016/j.gloplacha.2017.11.017
770 Colombo, N., Gruber, S., Martin, M., et al., 2018c. Rainfall as primary driver of discharge and solute export
771 from rock glaciers: the Col d'Olen rock glacier in the NW Italian Alps. Science of Total Environment, 639,
772 316-330. https://doi.org/10.1016/j.scitotenv.2018.05.068.
773 Cooper, R.J., Wadham, J.L., Tranter, M., et al., 2002. Groundwater hydrochemistry in the active layer of the
774 proglacial zone, Finsterwalderbreen, Svalbard. J. Hydrol., 269(3-4), 208-223.
775 https://doi.org/10.1016/S0022-1694(02)00279-2.
776 Duguay, M.A., Edmunds, A., Arenson, L.U., et al., 2015. Quantifying the significance of the hydrological
777 contribution of a rock glacier – A review. GEOQuébec 2015, 68th Can. Geotech. Conf. 7th Can. Permafr.
778 Conf., CD-Rom, Québec, QC, 20-23 September 2015.

779 Dumont, B., Gascoin, S., Hagolle, O., et al., 2021. Brief communication : evaluation of the snow cover
780 detection in the Copernicus High Resolution Snow & Ice Monitoring Service. The Cryosphere, 15(10),
781 4975-4980.
782 Engel, M., Penna, D., Bertoldi, G., et al., 2019. Controls on spatial and temporal variability in streamflow and
783 hydrochemistry in a glacierized catchment. Hydrology and Earth System Sciences, 23, 2041–2063.
784 https://doi.org/10.5194/hess-23-2041-2019.
785 Evans, S.G., S. Ge, Liang, S., 2015. Analysis of groundwater flow in mountainous, headwater catchments with
786 permafrost. Water Resour. Res., 51, 9564-9576. Doi: 10.1002/2015WR017732.
787 Gaspar, E., 1987. Modern trends in tracer hydrology. Ed. Emilian Gaspar, CRC Press Boca Raton, Fla.
788 Geiger, S.T., Daniels, J.M., Miller, S.N., et al., 2014. Influence of rock glaciers on stream hydrology in the La
789 Sal Mountains, Utah. Arctic, Antarctic, and Alpine Research, 46(3), 645-658.
790 https://dx.doi.org/10.1657/1938-4246-46.3645.
791 Haeberli, W., Schaub, Y., Huggel, C., 2017. Increasing risks related to landslides from degrading permafrost
792 into new lakes in deglaciating mountain ranges. Geomorphology, 293(B), 405-417.
793 https://doi.org/10.1016/j.geomorph.2016.02.009.
794 Haeberli, W., Hallet, B., Arenson, L., et al., 2006. Permafrost creep and rock glacier dynamics. Permafrost and
795 Periglacial Processes, 17(3), 189-214. https://doi.org/10.1002/ppp.561.
796 Haag, I.,Kern, U., Westrich, B., 2000. Assessing in-stream erosion and contaminant transport using the end-
797 member mixing analysis (EMMA). The Role of Erosion and Sediment Transport in Nutrient and
798 Contaminant Transfer. IAHS Publ. no, 263.
799 Halla, C., Blöthe, J.H., Tapia Baldis, C., et al., 2021. Ice content and interannual water storage changes of an
800 active rock glacier in the dry Andes of Argentina. The Cryosphere, 15, 1187–1213,
801 https://doi.org/10.5194/tc-15-1187-2021.
802 Harrington, J.S., Mozil, A., Hayashi, M., et al., 2018. Groundwater flow and storage processes in an inactive
803 rock glacier. Hydrological Processes, 32(20), 3070-3088. https://doi.org/10.1002/hyp.13248.
804 Harrington, J.S., Hayashi, M., Kurylyk, B., 2017. Influence of a rock glacier spring on the stream energy
805 budget and cold-water refuge in an alpine stream. Hydrological Processes, 31, 4719-4733. Doi:
806 10.1002/hyp.11391.

807 Hayashi, M., 2020. Alpine hydrogeology: the critical role of groundwater in sourcing the headwaters of the
808 world. Groundwater, 58(4), 498-510. https://doi.org/10.1111/gwat.12965.
809 Hugonnet, R., McNabb, R., Berthier, E., et al., 2021. Accelerated global glacier mass loss in the early twenty-
810 first century. Nature, 592, 726-732. https://doi.org/10.1038/s41586-021-03436-z.
811 Hudson, R., Fraser, J., 2008. Introduction to salt dilution gauging for streamflow measurement part IV: the
812 mass balance (or dry injection) method. Streamline Watershed Management Bulletin, 9(1), 6-12.
813 Huss, M., Bookhagen, B., Huggel, C., et al., 2017. Toward mountains without permafrost snow and ice. Earth'a
814 Future, 5(5), 418-435. https://doi.org/10.1002/2016EF000514.
815 Ilyashuk, B.P., Ilyashuk, E.A., Psenner, R., et al., 2018. Rock glaciers in crystalline catchments: Hidden
816 permafrost-related threats to alpine headwater lakes. Global Change Biology, 24(4), 1548-1562. Doi:
817 10.1111/gcb.13985.
818 Ilyashuk, B.P., Ilyashuk, E.A., Psenner, R., et al., 2014. Rock glacier outflows may adversely affect lakes:
819 lessons from the past and present of two neighboring water bodies in a crystalline-rock watershed.
820 Environmental Science & Technology, 2014, 48, 6192-6200. https://pubs.acs.org/doi/10.1021/es500180c.
821 Jin, H., Huang, Y., Bense, V.F., et al., 2022. Permafrost degradation and its hydrogeological impacts. Water,
822 14, 372. https://doi.org/10.3390/w14030372.
823 Jones, D.B., Harrison, S., Anderson, K., et al., 2018. Mountain rock glaciers contain globally significant water
824 stores. Scientific Reports, 8, 2834.
825 Jones, D.B., Harrison, S., Anderson, K., et al., 2019. Rock glaciers and mountain hydrology: A review. Earth-
826 Science Reviews, 193, 66-90. https://doi.org/10.1016/j.earscirev.2019.04.001.
827 Khamis, K., Brown, L.E., Milner, A.M., et al., 2015. Heat exchange processes and thermal dynamics of a
828 glacier-fed alpine stream. Hydrological Processes, 29, 3306–3317. https://doi.org/10.1002/hyp.10433.
829 Kopácek, J., Kana, J., Santruckova, H., et al., 2004. Chemical and biochemical characteristics of alpine soils
830 in the Tatra Mountains and their correlation with lake water quality. Water Air Soil Pollut., 153, 307–327.
831 https://doi.org/10.1023/B:WATE.0000019948.23456.14.
832 Krainer, K., Bressan, D., Dietre, B., et al., 2015. A 10,300-year-old permafrost core from the active rock glacier
833 Lazaun, southern Ötztal Alps (South Tyrol, northern Italy). Quaternary Research, 83, 324-335.

834 Krainer, K., Mostler, W., Spötl, C., 2007. Discharge from active rock glaciers, Austrian Alps: a stable isotope
835 approach. Austrian Journal of Earth Sciences, 100, 102-112.
836 Krainer, K., Mostler, W., 2002. Hydrology of active rock glaciers: examples from the Austrian Alps. Arctic,
837 Antarctic, and Alpine Research, 34(2), 142-149.
838 Kralik, M., 2015. How to estimate mean residence times of groundwater. Procedia Earth and Planetary Science,
839 13, 301-306. https://doi.org/10.1016/j.proeps.2015.07.070.
840 Longinelli, A., Selmo, E., 2003. Isotopic composition of precipitation in Italy: a first overall map. Journal of
841 Hydrology 270, 75-88. DOI: 10.1016/S0022-1694(02)00281-0.
842 Magnusson, J., Jonas, T., Kirchner, J.W., 2012. Temperature dynamics of a proglacial stream: Identifying
843 dominant energy balance components and inferring spatially integrated hydraulic geometry. Water
844 Resources Research, 48, W06510. https://doi.org/10.1029/2011WR011378.
845 Mania, I., Gorra, R., Colombo, N., et al., 2018. Prokaryotic diversity and distribution in different habitats of
846 an alpine rock glacier-pond system. Microbial Ecology, 78(1), 70-84. Doi: 10.1007/s00248-018-1272-3.
847 Mari, S., Scapozza, C., Pera, S., et al., 2013. Prove di multitracciamento di ghiacciai rocciosi e ambienti
848 periglaciali nel Vallon de Réchy (VS) e nella Valle di Sceru (TI). Bollettino della Società ticinese di scienze
849 naturali, 101, 13-20. ISSN 0379-1254.
850 Michel, A., Schaefli, B., Wever, N., et al., 2022. Future water temperature of rivers in Switzerland under
851 climate change investigated with physics-based models. Hydrol. Earth Syst. Sci., 26, 1063-1087.
852 https://doi.org/10.5194/hess-26-1063-2022.
853 Michel, A., Brauchli, T., Lehning, M., et al., 2020. Stream temperature and discharge evolution in Switzerland
854 over the last 50 years: annual and seasonal behaviour. Hydrol. Earth Syst. Sci., 24, 115-142.
855 https://doi.org/10.5194/hess-24-115-2020.
856 Millar, C.I., Westfall, R.D., Delany, D.L., 2013. Thermal and hydrologic attributes of rock glaciers and
857 periglacial talus landforms: Sierra Nevada, California, USA. Quaternary International, 1-12.
858 https://dx.doi.org/10.1016/j.quaint.2012.07.019.
859 Munroe, J.S., 2018. Distribution, evidence of internal ice, and possible hydrologic significance of rock glaciers
860 in the Uinta Mountains, Utah, USA. Quaternary Research, 90, 50-65. https://doi.org/10.1017/qua.2018.24.

Niedrist, G.H., Füreder, L., 2020. Real-time warming of Alpine streams: (re)defining invertebrates' temperature preferences. River Res. Applic., 2021, 37, 283-293. Doi: 10.1002/rra.3638.

Penna, D., van Meerveld, H.J., 2019. Spatial variability in the isotopic composition of water in small catchments and its effect on hydrograph separation. Wiley Interdisciplinary Reviews Water, 6(5). https://doi.org/10.1002/wat2.1367.

R Development Core Team, 2022. R: A language and environment for statistical computing. R Foundation for Statistical Computing, Vienna, Austria. https://www.R-project.org/

Rogger, M., Chirico, G.B., Hausmann, H., et al., 2017. Impact of mountain permafrost on flow path and runoff response in a high alpine catchment. Water Resour. Res., 53, 1288-1308. Doi: 10.1002/2016WR019341.

Rogora, M., Somaschini, L., Marchetto, A., et al., 2020. Decadal trends in water chemistry of Alpine lakes in calcareous catchments driven by climate change. Sci. Total Environ., 708, 135180. https://doi.org/10.1016/j.scitotenv.2019.135180.

Salerno, F., Rogora, M., Balestrini, R., et al., 2016. Glacier melting increases the solute concentrations of Himalayan glacial lakes. Environ. Sci. Technol., 50(17), 9150–9160, https://doi.org/10.1021/acs.est.6b02735.

Scapozza, C., Deluigi, N., Bulgheroni, M., et al., 2019. Assessing the impact of ground ice degradation on high mountain lake environments (Lago Nero catchment, Swiss Alps). Aquatic Sciences, 82(5), 1-16. https://doi.org/10.1007/s00027-019-0675-7.

Seppi, R., Zanoner, T., Carton, A., et al., 2015. Current transition from glacial to periglacial processes in the Dolomites (South-Eastern Alps). Geomorphology, 228, 71-86. https://doi.org/10.1016/j.geomorph.2014.08.025.

Schmid, M.-O., Gubler, S., Fiddes, J., et al., 2012. Inferring snowpack ripening and melt-out from distributed measurements of near-surface ground temperatures. The Cryosphere, 6, 1127-1139. Doi: 10.5194/tc-6-1127-2012.

Schlosser, P., Stute, M., Dörr, H., et al., 1988. Tritium/3He dating of shallow groundwater. Earth and Planetary Science Letters 89, 353–362.

Schnegg, P.A., 2002. An inexpensive field fluorometer for hydrological tracer tests with three tracers and turbidity measurement. Groundwater and Human Development.

Sileo, N. R., Dapeña, C., Trombotto Liaudat, D., 2020. Isotopic composition and hydrogeochemistry of a periglacial Andean catchment and its relevance in the knowledge of water resources in mountainous areas. Isotopes in Environmental and Health Studies, 56(5-6), 480-494. https://doi.org/10.1080/10256016.2020.1814278.

Somers, L.D., Gordon, R.P., McKenzie, J.M., et al., 2016. Quantifying groundwater-surface water interactions in a proglacial valley, Cordillera Blanca, Peru. Hydrological Processes, 30, 2915–2929. https://doi.org/10.1002/hyp.10912.

Spence, J., Telmer, K., 2005. The role of sulfur in chemical weathering and atmospheric CO_2 fluxes: evidence from major ions, $\delta^{13}C_{DIC}$, and $\delta^{34}S_{SO4}$ in rivers of the Canadian Cordillera. Geochim. Cosmochim. Acta, 69(23), 5441–5458. https://doi.org/10.1016/j.gca.2005.07.011.

Steingruber, S.M., Bernasconi, S.M., Valenti, G., 2020. Climate change-induced changes in the chemistry of a high-Altitude mountain lake in the central Alps. Aquatic Geochemistry. https://doi.org/10.1007/s10498-020-09388-6.

Solomon, D. K., Poreda, R. J., Cook, P. G., et al., 1995. Site Characterization Using 3H/3 He Ground-Water Ages, Cape Cod, MA. Groundwater, 33(6), 988-996. https://doi.org/10.1111/j.1745-6584.1995.tb00044.x

Suckow, A., 2014. The age of groundwater–Definitions, models and why we do not need this term. Applied Geochemistry, 50, 222-230. https://doi.org/10.1016/j.apgeochem.2014.04.016

Tenthorey, G., 1992. Perennial névés and the hydrology of rock glaciers. Permafrost and Periglacial Processes, 3, 247-252. https://1045-6740/92/030247-06$08.00

Thies, H., Nickus, U., Tessadri, R., et al., 2018. Peculiar arsenic, copper, nickel, uranium, and yttrium-rich stone coatings in a high mountain stream in the Austrian Alps. Austrian J. Earth Sci., 110(2). https://doi.org/10.17738/ajes.2017.0012.

Thies, H., Nickus, U., Tolotti, M., et al., 2013. Evidence of rock glacier melt impacts on water chemistry and diatoms in high mountain streams. Cold Reg. Sci. Technol., 96, 77-85. https://doi.org/10.1016/j.coldregions.2013.06.006.

Tranter, M., Sharp, M.J., Brown, G.H., et al., 1997. Variability in the chemical composition of in-situ subglacial meltwaters. Hydrologic Processes, 11, 59–77. https://doi.org/10.1002/(SICI)1099-1085(199701)11:1<59::AID-HYP403>3.0.CO;2-S

Ulloa-Cedamanos, F., Probst, A., Moussa, I., et al., 2021. Chemical weathering and CO2 consumption in a multi-lithological karstic critical zone: Long term hydrochemical trends and isotopic survey. Chemical Geology, 585, 120567. https://doi.org/10.1016/j.chemgeo.2021.120567

van Vliet, M.T.H., Franssen, W.H.P., Yearsley, J.R., et al., 2013. Global river discharge and water temperature under cliamte change. Global Environmental Change, 23, 450-464. https://doi.org/10.1016/j.gloenvcha.2012.11.002.

Viviroli, D., Kummu, M., Meybeck, M., et al., 2020. Increasing dependence of lowland populations on mountain water resources. Nature Sustainability, 3, 917-928. https://doi.org/10.1038/s41893-020-0559-9.

Wagner, T., Kainz, S., Helfricht, K., et al., 2021a. Assessment of liquid and solid water storage in rock glaciers versus glacier ice in the Austrian Alps. Science of the Total Environment, 800. https://doi.org/10.1016/j.scitotenv.2021.149593.

Wagner, T., Kainz, S., Krainer, K., et al., 2021b. Storage-discharge characteristics of an active rock glacier catchment in the Innere Ölgrube, Austrian Alps. Hydrological Processes, 35. https://doi.org/10.1002/hyp.14210.

Wagner, T., Brodacz, A., Krainer, K., et al., 2020. Active rock glaciers as shallow groundwater reservoir, Austrian Alps. Grundwasser – Zeitschrift der Fachsektion Hydrogeologie. https://doi.org/10.1007/s00767-020-00455-x.

Westoby, M.J., Brasington, J., Glasser, N.F., et al., 2012. "Structure-from-Motion" photogrammetry: A low-cost, effective tool for geoscience applications. Geomorphology, 179. https://doi.org/10.1016/j.geomorph.2012.08.021.

Williams, M.W., Knauf, M., Cory, R., et al., 2007. Nitrate content and potential microbial signature of rock glacier outflow, Colorado Front Range. Earth Surface Processes and Landforms, 32(7). https://doi.org/10.1002/esp. 1455.

Williams, M.W., Knauf, M., Caine, N., et al., 2006. Geochemistry and source waters of rock glacier outflow, Colorado front range. Permafrost and Periglacial Processes, 17, 13-33. Doi: 10.1002/ppp.535.

Winkler, G., Wagner, T., Krainer, K., et al., 2018. Hydrogeology of rock glaciers – storage capacity and drainage dynamics – an overview. In: Sychev, V.G., Mueller, L. (Eds.), Novel Methods and Results of

944 Landscape Research in Europe, Central Asia and Siberia. Volume 2, FGBNU "VNII agrochimii", Moscow,
945 Russia, pp. 329-334.
946 Winkler, G., Wagner, T., Pauritsch, M., et al., 2016. Identification and assessment of groundwater flow and
947 storage components of the relict Schöneben rock glacier, Niedere Tauern Range, Eastern Alps (Austria).
948 Hydrogeol J., 24, 937-953. Doi: 10.1007/s10040-015-1348-9.
949 Zemp, M., Frey, H., Gärtner-Roer, I., et al., 2015. Hystorically unprecedented global glacier decline in the
950 early 21st century. Journal of Glaciology, 61(228), 745-762. Doi: 10.3189/2015JoG15J017.